Orifice Coefficients for an Asymmetrical Flow into a Slot

Thesis by
Kurt Arthur Andrews

In Partial Fulfillment of the Requirements
for the
Engineer's Degree

California Institute of Technology
Pasadena, California
1989
(Submitted September 1, 1988)

Acknowledgements

I give special thanks to one of the finest persons I have ever had the privilege to be associated with, my advisor, Professor R.F. Sabersky. His insight and direction were irreplaceable throughout my stay at CALTECH and I appreciate the assistance he has extended in all aspects of my endeavors. I thank also Professors A.J. Acosta and J.K. Knowles for their continuing interest in my research and welfare. I feel indebted to Professor C.E. Brennen, who generously allowed me the use of the HDA Test Stand and offered his assistance throughout the experiment.

Appreciation is sent to Joe Fontana and Rich Eastvedt of the W.M. Keck Laboratory of Hydraulics and Water Resources, who offered invaluable assistance in the design, fabrication and construction of the experimental device. Furthermore, I would like to acknowledge the help of Richard Arrieta, a student, who assisted in building and assembling the apparatus, and in collecting data.

Finally, deepest thanks go to my family for their understanding and encouragement over the years of my formal education. I dedicate this thesis with love to my wife, Marcia Andrews, whose assistance, inspiration and tolerance were greatly appreciated.

Abstract

The purpose of this investigation is to determine what percentage, if any, of a freestream velocity head is recovered by the flow through a slot. In this experiment, fluid is drawn through a slot placed perpendicular to a passing flow. This project addresses orifice coefficients, a classic subject, which has been thoroughly investigated. However, unlike most of the previous experiments measuring orifice or resistance coefficients, the flow approaching the orifice, or slot in this case, is not symmetrical. Mainstream flow rate and orifice flows are explored systematically over a fairly wide range. The primary motivation is to gain a better understanding of the fluid dynamics associated with small orifices in the presence of a passing flow.

Contents

List of Figures

List of Tables

Nomenclature

A	Area
a	width of separation bubble
b	length of separation bubble
C_d	orifice coefficient, $\frac{1}{\sqrt{C_p}}$
C_p	slot pressure drop coefficient, $\Delta p/(\frac{1}{2}\rho u_s^2)$
d	pipe inner diameter
g	gravitational constant
p	pressure
q	volumetric flow rate
r	pipe radius
Re_d	pipe Reynolds number, $\frac{Ud}{\nu}$
Re_w	slot Reynolds number, $\frac{u_s w}{\nu}$
Re_x	flat plate Reynolds number, $\frac{Ux_l}{\nu}$
h	slot depth
T	temperature
U	freestream velocity in the pipe upstream of slot
U_m	bulk velocity in pipe upstream of slot
u_s	bulk slot suction velocity
x	streamwise coordinate in pipe
y	cross-stream coordinate
z	manometer reading (height)
δ	boundary-layer thickness
Δp	slot pressure drop
ν	fluid kinematic viscosity

ρ density of fluid

Subscripts

p in the pipe

s in the slot

o in the orifice chamber

Chapter 1

Introduction

The study of flows through pipes and orifices is as old as the science of fluid mechanics. Pressure-loss coefficients have been determined for a wide variety of orifices operating over a wide range of flow velocities. In the vast majority of cases, these experimentally derived orifice coefficients are useful only when the flow approaching the orifice is symmetric. There is almost no information about flows where the orifice inlet is perpendicular to a passing flow. It is this problem that is being addressed here.

As an example in which this type of orifice flow occurs, one may cite the problem of boundary-layer control by suction or more specifically by laminar-flow control (LFC). By delaying the onset of turbulence, it is possible to reduce a vehicle's skin friction drag. One of the more promising methods involves removing a portion of the boundary layer by suction. The concept is based upon reducing the size of the boundary layer and thus its sensitivity to disturbances that lead to turbulence. With the use of suction, the boundary layer can be reduced and the onset of turbulence delayed. In this manner, friction drag can be reduced. Although the literature is replete with various analyses and research on this subject, there is little written about the pressure drop that occurs across the suction orifices. Information on orifice coefficients is needed to allow the designer to predict the power required to

control the boundary layer by suction.

1.1 Background and Prior Work

By far the most comprehensive review on orifice coefficients is given by the Russian author I. Idel'Chik [9]. A second edition, edited by E. Fried, is the most comprehensive and also contains an extensive bibliography. This book covers a wide variety of orifices under varying conditions. For symmetrical inlet flows, Idel'Chik notes that three specific flow regimes exist, which are analogous to pipe flow. In the purely laminar region, C_d depends only on the Re_w in the orifice. In the transition region, which is applicable to this study, C_d is a function of the geometry and Re_w. While in the fully turbulent region, C_d is a function of geometry and virtually independent of Re_w. Although the three regions are weakly dependent on the orifice geometry, typically they are quantified as follows [9]:

$Re_w \leq 30$	laminar
$30 < Re_w \leq 10^4$	transition
$10^4 < Re_w$	turbulent

The 1986 edition by Idel'Chik also contains results from V.I. Khanzhonkov [10], who is one of the few who conducted measurements of orifice coefficients influenced by a passing stream. His results for $Re_w > 10^4$ and thin orifices are of interest, though not fully applicable to the present study. He concluded that for small velocities of the passing steam ($U \ll u_s$), the resistance through the orifice decreased, but for $U \gg u_s$ the resistance increased.

H. Schlichting [15] provides a good introduction to the subject of boundary-layer suction, which is of incidental interest. Additional information is given by

N. Gregory [7] and W. Pfenninger [13], who have carried out extensive experiments utilizing suction through slots to reduce drag. P. Chang [3] discusses and provides an extensive bibliography on the use of suction on airfoils to prevent boundary-layer separation. Yet none of these authors have published measurements addressing the pressure drop across the orifice.

A.S.W. Cornelius and K.C. Thomas [16] have done experiments similar to the present one. They conducted tests in a water channel, but with slower freestream velocities ($U \leq 2$ m/s), lower slot Reynolds numbers ($Re_w \leq 300$), and larger slot width ($w \geq 2.7$ mm) than in this experiment. They were able to visualize the flow, and under certain conditions, they detected a "separation bubble" as illustrated in Fig. 1.1. The emphasis of their research was to determine the nature of the separation bubble. Using a small stream of fluorescent dye, they were able to measure the dimensions, a and b, of the separation bubble. Incidental to this, they measured the pressure difference across the slot. In their experiments only a small portion of the boundary layer actually entered the slot and, therefore, they were able to characterize the approaching flow by a simple, linear velocity gradient (dU/dy). Consequently, the flow in the boundary layer was replaced by a uniform shear. Within this simplified flow field, the strength of this velocity gradient defines the flow in the vicinity of the slot. This led to the development of dimensionless parameters used to describe the simplified flow field. However, in the present experiment, the slot flow rate varies over a greater range and these simplifications do not necessarily apply.

Interestingly, they produced results hinting that the minimum Δp for a given flow rate does not occur at zero freestream velocity, where Δp is defined as follows:

$$\Delta p = p_p - p_o \, .$$
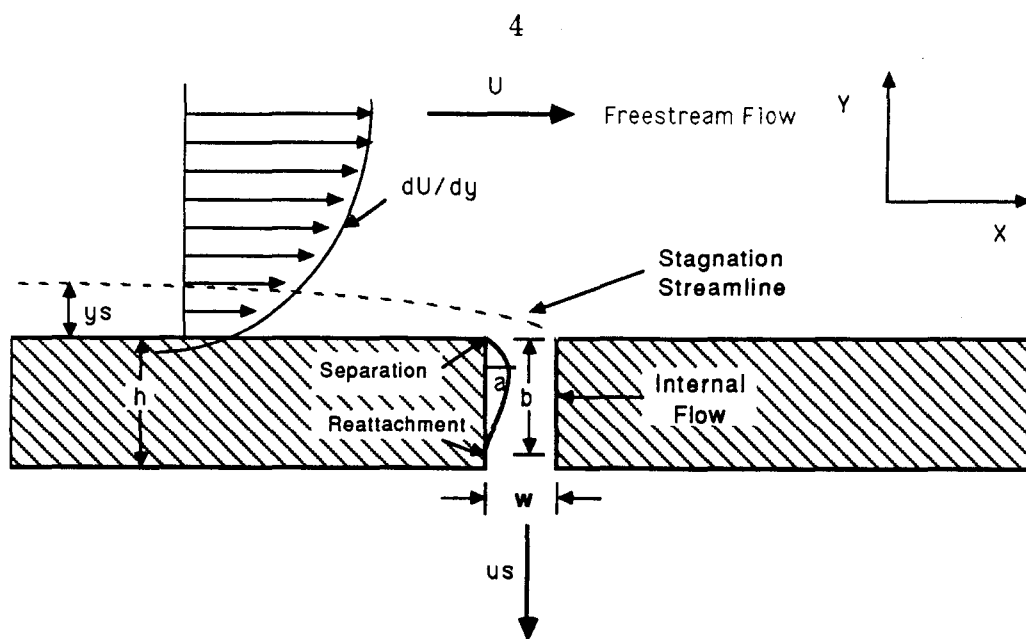
Figure 1.1: Configuration of a laminar-flow suction slot.

Both p_p and p_o are static pressures on opposite sides of the orifice. Thomas and Cornelius [16, page 795] reasoned:

> Apparently, there is some nonzero external velocity gradient that minimizes the pressure drop across the slot. This arises because, unlike the case of zero shear flow , the external flow now has some average momentum that actually aids in driving the fluid into the slot, with minimal acceleration or viscous losses being associated with the downward turning of the flow. On the other hand, as the shear is further increased, the suction flow comes from a region closer to the wall and must be turned more suddenly and sharply so as to be able to enter the slot.

J. Brandeis [2] offers a numerical solution to the slot flow problem. Using compressible, boundary-layer equations in the viscous region and the incompressible Navier-Stokes model applied in the slot, he solves the two regions and matches them interactively. His results, however, do not include values for C_p. Similarly,

S. Hoerner [8] discusses the energy requirements associated with boundary-layer control on airfoils through suction, but does not discuss pressure-loss coefficients.

1.2   Scope of the Research

The present investigation was designed to measure the pressure drop (Δp) across a small orifice or slot at various slot and freestream fluid velocities, and to determine the effect of stream velocity on flow through the slot. We were particularly interested in determining whether or not any of the velocity head in the pipe is recovered. In order to address these goals, mainstream and orifice flow rates were explored systematically over a fairly wide range.

Chapter 2

System Design

2.1 Design Requirements and Problems

The present experiment is exploratory in nature. Therefore, a simple and relatively inexpensive installation was designed sufficient to meet the goals of the research. In this apparatus the freestream flow is represented by the flow in a pipe, and fluid is withdrawn through a slot in the pipe wall. For the conditions in this experiment, the boundary layer remained small compared to the pipe radius, and the flow approximated reasonably well the flow over a flat plate. The assumption that the boundary layer is thin is evaluated in more detail in Appendix A.

The apparatus had to have an adjustable slot and a reservoir into which the fluid passing through the slot could be discharged. It was first suggested that a 2 cm inner diameter pipe be used with a slot placed 10 cm from the pipe entrance. From these initial dimensions it was determined that a pump of at least 1 HP would be needed. Fortunately, a suitable test stand was available and could be adapted for the present experiments. This test stand depicted in Fig. 2.5 consisted of a system of valves, a filter, a rotor Flometer and a 1.5 HP centrifugal pump. The flow meter was calibrated to ensure that it was still operating properly. It was determined that this system could pump over 60 GPM, which would generate a flow over 8 m/s in

a 2.54 cm pipe. At this flow rate $Re_d = 2 \times 10^5$, implying turbulent flow if the flow were fully developed. The length Reynolds number, $Re_x = 8 \times 10^5$, however, predicts a flow near the transition between laminar and turbulent flow. These flow conditions were considered to be acceptable for our purpose, and it was decided that the existing test stand could be utilized.

To avoid using another power source to draw off fluid, the test section was to be operated at a pressure greater than atmospheric. By placing the test section on the pressure side of the pump, the fluid could be vented through a slot simply by opening a valve to atmosphere. The drawback to this design is that, typically, it is more difficult to maintain a laminar flow on the pressure side of a pump since the freestream turbulence induced by the pump is carried forward in the system.

In order to maintain laminar flow, a smooth pipe surface was desired. Furthermore, to allow for flow visualization, a clear material was required. Therefore, most of the experimental apparatus was built out of Lucite plastic. This material had the added benefits of being easy to machine, relatively inexpensive, noncorrosive and, most importantly, very smooth when polished.

2.2 Experimental Setup

For ease of discussion the apparatus is divided into five major parts: the settling chamber, the contraction, the pipe and test section, the reservoir, and the test stand. These are depicted in Fig. 2.1
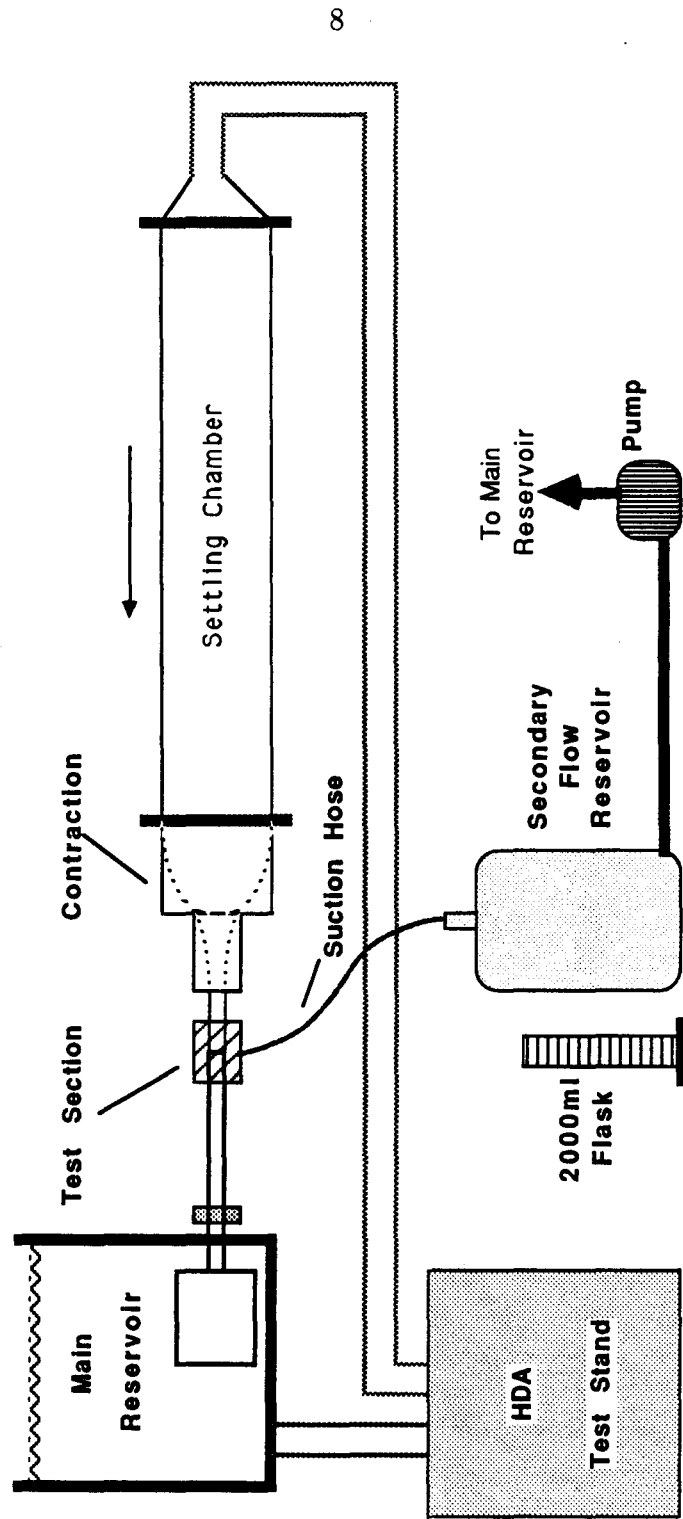
Figure 2.1: A Schematic Diagram of the System.
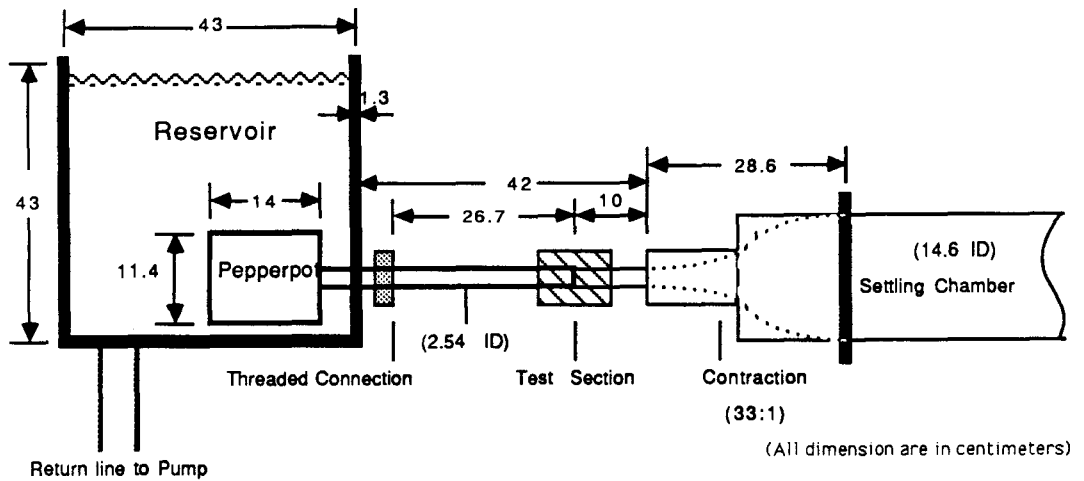
Figure 2.2: An Overview of the Apparatus.

2.2.1 The Settling Chamber

To develop a laminar flow just prior to the test section, a settling chamber was required. Settling chambers are used in most wind and water tunnels. Therefore, a wealth of literature exists on their construction. The most detailed recent study is by Loehrke and Nagib [12]. From this study and that of Barker and Gile [1], the following design considerations were formulated. The flow within the settling chamber should be no greater than 0.5 m/s and should have interspersed throughout a combination of turbulence-reducing mechanisms. Readily available was a 14.6 cm inner diameter, Lucite tube that carried a flow rate of less than 0.25 m/s at the maximum test velocities. The settling chamber was 1.22 m long and was made up of two sections, although it had been designed to be divided into three sections if required. The smaller, 0.3048 m section was to be cut in half and fitted with turbulence-reducing screens. However, after installing turbulence manipulators, which included a wire screen, porous "horse hair," and honeycomb material as depicted in Fig. 2.3,
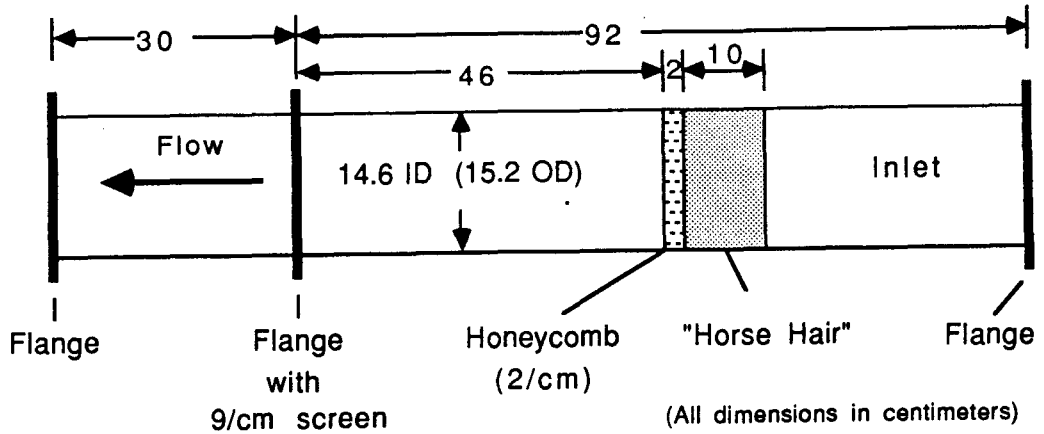
Figure 2.3: The Settling Chamber.

the flow appeared to be steady, uniform, and parallel. Therefore, no further cuts were made to the settling chamber.

2.2.2 The Contraction

The design of an axisymmetric contraction that would smoothly accelerate the flow from the settling chamber to the test section was critical. It was important that boundary-layer separation not occur at the inlet to the test section. G. Chmielewski [4] has shown with potential flow analysis how various contraction parameters affect inlet boundary-layer separation. From this paper Barker and Gile [1] designed two contractions for their work with high-speed laminar flows. Their contraction ratio (A_{inlet}/A_{outlet}) was 34.6:1, which was approximately the same as the contraction ratio (33:1) needed for the present installation. Accordingly the contraction section was patterned after that described by Barker and Giles. The contraction was 0.267

m long, with a length-to-diameter ratio of 1.83. It was carved on a lathe out of two 3-inch pieces of Lucite plastic.

2.2.3 The Test Section

Attached to the contraction was a 10.16 cm long, 2.54 cm inner diameter Lucite pipe. The union of the inner surface of the pipe with the contraction has a measurable step of less than 0.15 mm. Connected to the pipe by cement is the test section as shown in Fig. 2.4. The test section was carved on a lathe out of a 8.255 cm by 7.62 cm (3 inch) diameter cylinder of Lucite. The slot in the test section was formed by the space between the ends of two plastic tubes. The first tube has been described above and the second is attached to the test section by a threaded fitting. By rotating the threaded tube, the slot width (w) could be adjusted. There are 9.45 threads per cm (24 threads per inch); therefore, a 360 degree turn produced a 1.058 mm movement. The play in the threads perpendicular and parallel to the tube was negligible. However, it was possible to measure a 0.05 mm movement on the end of the test section furthest from the threads when applying a bending moment to the test section and the threaded tube. This play could be induced only by strong bending. The apparatus would return to its previous position, once the force had been removed. Therefore, the error induced by the play in the threads is considered negligible.

The original Lucite pipe was out of round by as much 0.4 mm and the two tubes were not exactly the same diameter. Therefore, they were machined on the lathe to insure a good match at the slot. The measurable step at the slot was 0.1 mm. It was attempted to keep the slot edges sharp, but some of the sharpness was lost during the polishing process.
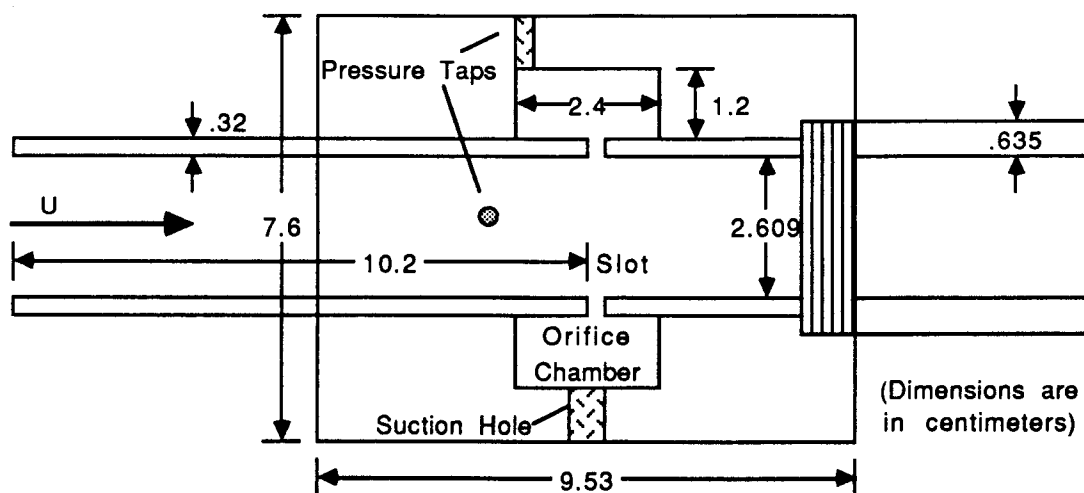
Figure 2.4: The Test Section

The test section had a 1.17 cm deep by 2.41 cm long orifice chamber. The fluid escaped through a 0.32 cm ($\frac{1}{8}$ inch) thick (h) slot into the chamber. On the bottom of this annular chamber was a threaded 0.95 cm hole, which was connected by means of a rubber hose to a Dwyer flow gauge and valve, which controlled the amount of fluid being suctioned off. From the flow gauge the water went to either a 2000 ml EXAX flask or a 15 gallon reservoir, depending on the application. This reservoir was attached by a rubber hose to a FLOTEC F2P4-1062 pump, which provided means of returning the suctioned fluid to the main reservoir. With this system it was possible to continually withdraw fluid through the suction slots.

2.2.4 The Reservoir

The test section assembly was attached to the reservoir by a threaded, quick-disconnect type fitting as shown in Fig. 2.1. Inside the Lucite plastic reservoir was a 14 cm long by 11.43 cm outer diameter "pepperpot." Its purpose was to diffuse the high-velocity head coming out of the test section tube by dispensing the

fluid radially. This device had 16 holes, 0.8 cm in diameter. The 52 liter open air reservoir had a 6.35 cm drainage hole in its bottom, which was used as a return line to the pump.

2.2.5 The Test Stand

The test stand, shown in Fig. 2.5 consisted of 13 valves to control the flow, most of which were not needed for this experiment, a 1.5 HP centrifugal pump, a MK 509 self-powered analog Flometer and a MK 515 Paddlewheel Flosensor. Control of the flow rate was achieved by adjusting two valves. One valve controlled the flow rate through the pipe, while the other valve controlled the flow in an internal feedback loop within the test stand. The feedback loop allowed the pump to continue operating near its designed flow level independent of the flow rate through the test loop. This feature created a steadier flow, especially for the slower test-loop flows, than would have been possible had the flow been controlled by only one valve. The test stand was attached to the test loop by 20"-80 PVC tubing. The maximum flow obtained in this configuration was just over 6 m/s or 50 GPM.
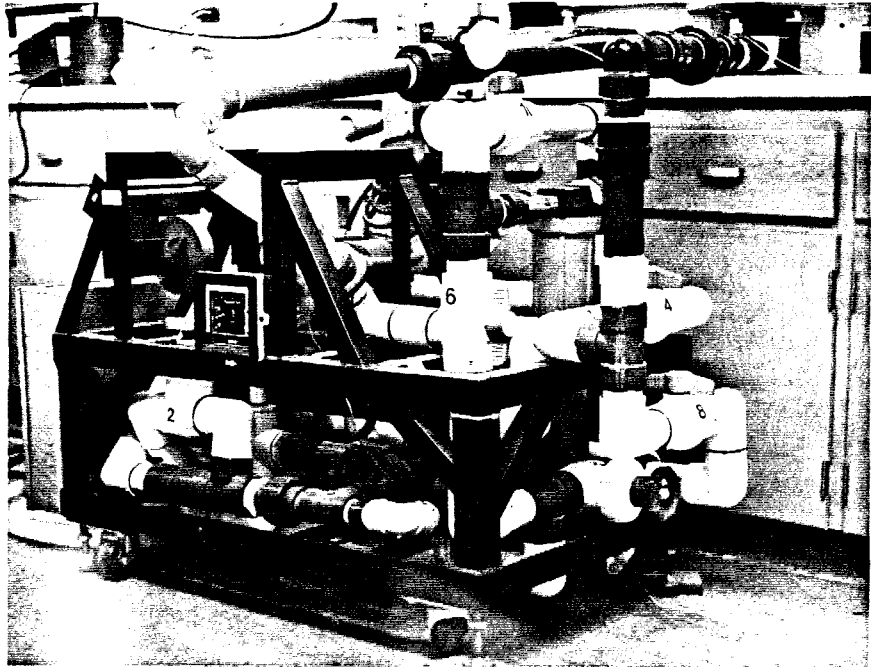
Figure 2.5: The test stand was designed and built by Gruczelak and Associates, Inc. for a previous experiment.

Chapter 3

Instrumentation and Calibration

For this experiment there are six variables of importance: the slot width (w), the volumetric flow rate in the pipe (q_p), the volumetric flow rate through the slot (q_s), the difference between the static pressure in the pipe at the slot and inside the orifice chamber (Δp). From these quantities, other parameters are determined and will be discussed further.

The slot width was adjusted by turning the threaded tube a predetermined amount and was checked by the use of feeler gages for all sets of data. The commercially made feeler gauges were available in sizes, $0.005''$, $0.010''$, and $0.020''$. With a micrometer, it was determined that normal deviation for the feeler gauges was ± 0.02 mm ($\pm 0.001''$). This is also the precision with which the slot was measured. Allowing for other factors such as swelling or shrinking of the Lucite because of contact with water, or expansion because of heating, it was first conservatively estimated that the slot distance was accurate to within 0.1 mm for the largest slot-width.

In order to evaluate the accuracy of this measurement technique, and the effects of swelling and heating on the plastic, the slot distance was reset and remeasured on various days and conditions. Data were taken and compared to previous data and usually the results were similar. Differences in the results did occur, however, for the smallest slot width. A re-estimation showed that the slot-width

measurement error was about ±0.02 mm.

The volumetric flow rate was determined with the use of the MK 515 Paddle-wheel Flosensor installed on the test stand. Although a Signet Scientific MK 509 self-powered analog Flometer was part of the test stand, it was not used. In this experiment the MK 515 Flosensor was connected to a digital, frequency counter for greater accuracy. The Flosensor and frequency counter were calibrated by pumping 20 gallons out of a calibrated reservoir into a container. For each data point the time and the reading from the frequency counter were recorded. This calibration data are plotted in Fig. 3.1. The straight line in Fig. 3.1 is plotted from the equation $q = 1.79f$, which is the calibration formula recommended by Signet Scientific for $2'' - 80$ pipe. In this formula q is the volumetric flow (GPM) and f is the frequency (Hz). The manufacturer claims accuracy to within ±2%. Fig. 3.1 shows that there may be some deviation from the suggested values near the top of this range. Nevertheless, the straight-line equation was believed to be sufficiently accurate for the flow-rate range of this experiment.

The error associated with determining the flow rate in the pipe came from two major sources. One is the calibration of the Flosensor, previously discussed, and the other is the random error associated with the meter readings. Although the frequency counter was set for its longest counting interval of ten seconds, there was still a fairly significant variation (±.8 Hz or ±6%) in the individual readings. The velocities given for each set of data, therefore, were derived by averaging the frequencies taken.

The volumetric flow rate in the slot was determined by timing the flow into a 2000 ml flask. The flask was calibrated by weighing the flask, first dry and then wet, and then subtracting the difference to derive the weight of the fluid. Assuming
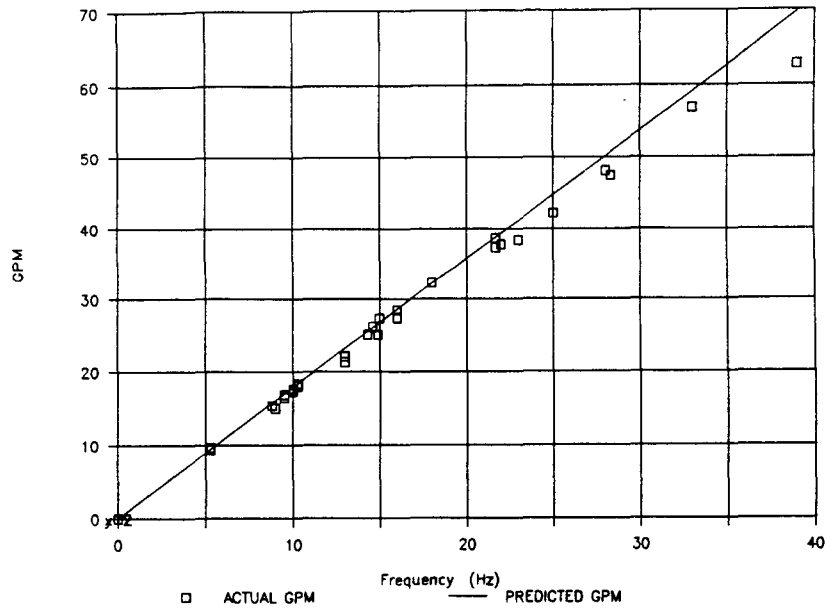
Figure 3.1: Comparison of flow rate to the Flosensor frequency.

the density of the water to be 0.998 gm/l, it was found that the weight of the fluid

corresponded to within ±1% to the measured volume.

An air-water manometer was used to measure the pressure difference (Δp). It

had a length of 80 cm (2.6 ft) high and could be pressurized with air from a common

chamber above. This manometer was chosen, since it offered the greatest precision

without the constant calibration requirements associated with electrical pressure

transducers. Especially, since the pressure differences being measured ranged from

less than 0.5 cm to 80 cm water (49 to 7840 N/m^2). An inherent problem with

the manometer is the random error associated with reading the meniscus. The

manometer was equipped with mirrors behind the glass tubes; however, at high-

pipe velocity the manometer levels fluctuated by as much as ±0.5 cm. Taking

these factors into account, the error associated with readings from the manometer

is estimated to be less than ±1.5 mm.

The static pressure was measured from a tap 3.2 cm upstream of the slot. An

upstream location was chosen to avoid the influence of the discharge through the

slot. The pressure tap consisted of a .7 mm hole, 5 mm deep from the inner surface, which joined a 4 mm hole to the outer surface. A pressure tap was threaded into the hole and connected to the water manometer by small plastic tubing.

The pressure tap for measuring the static pressure inside the orifice had to be located with some care. We wanted to ensure that the tap was not recovering some of the slot flow velocity head. High-velocity flows, up to 4.5 m/s, enter the orifice chamber and are turned downward toward the suction hole. Two positions for the pressure tap were tried. The first was directly opposite the slot and the second, in a corner as depicted in Fig. 2.4. It was felt that at high-slot flows the position opposite the slot might be measuring a partial stagnation pressure instead of a static pressure. Therefore, for the data presented, the second position was used. It was later determined, by comparing data taken under both circumstances, that this change made little difference in the results.

Chapter 4

Experimental Procedure

4.1 Constant Pipe Flow

Data were collected in groups by slot width using the following procedure. The slot width and the pipe-flow rate would be set and a reading would be taken on the manometer for zero-slot flow. Although the pressure drop across the slot (Δp) should have been very close to zero, for reasons not completely understood, this was not always the case. Typically, $\Delta p = p_o - p_p$ varied from $-.3$ to $+1$ cm, with the larger variations occurring at higher velocities. These variations indicate that there were some small imperfections in the manufacture of the pressure taps or the slot.

Using the valve on the Dwyer adjustable flow gauge, the flow from the slot was set, usually, for the first reading, to full open or max flow. The rubber tube from the Dwyer valve drained into the white plastic floor reservoir depicted in Fig. 2.1. In order to measure the flow rate through the slot (q_s) the tube would be moved from the floor reservoir to the EXAX flask, where the filling of the 2000 ml flask was timed. The rubber hose would then be returned to the floor reservoir, where the water was pumped back to the main reservoir at a rate commensurate with the slot flow. The goal was to keep the main reservoir level constant by varying the output of the small return pump. The Dwyer gauge was used to confirm that the flow was

steady and not affected by the movement of the hose.

The manometer would be monitored during this entire process, and when it equilibrated, a reading would be taken. A drawback of using the water manometer was that it often took a long time for the water column to reach its equilibrium level, in this case sometimes up to 5 minutes. This problem was alleviated, at least partially, by keeping a flow in the slot at all times. When the next data point was to be taken, and the flow in the slot was adjusted accordingly, the change in the manometer would be small.

For each data point, four values were recorded: the frequency from the counter, the time to fill the 2000 ml flask, the temperature from the reservoir thermometer, and the reading in feet from the manometer. By changing the slot flow slightly, another data point would be generated. Typically, between 10 to 15 data points would be taken for a given flow in the pipe. Upon completion of a set of data, the slot flow would then be set to zero and another reading taken on the manometer. This, in turn, would be compared to the first reading and the mean used to compute other values. Finally, the set of data for a given pipe flow was completed. In some cases, for comparison, data were repeated later. The valves on the test stand would be adjusted for a new pipe flow and the same procedure repeated. For each slot width, five sets of data were taken, each corresponding to a different pipe flow.

4.2 Constant Orifice Flow

For ease of comparison to data by Thomas and Cornelius [16], and to check data points taken by the normal method, an alternate method was sometime used. In this method the slot flow was held constant while the pipe flow was allowed to vary within each data set. This was achieved by adjusting the Dwyer flow gauge to
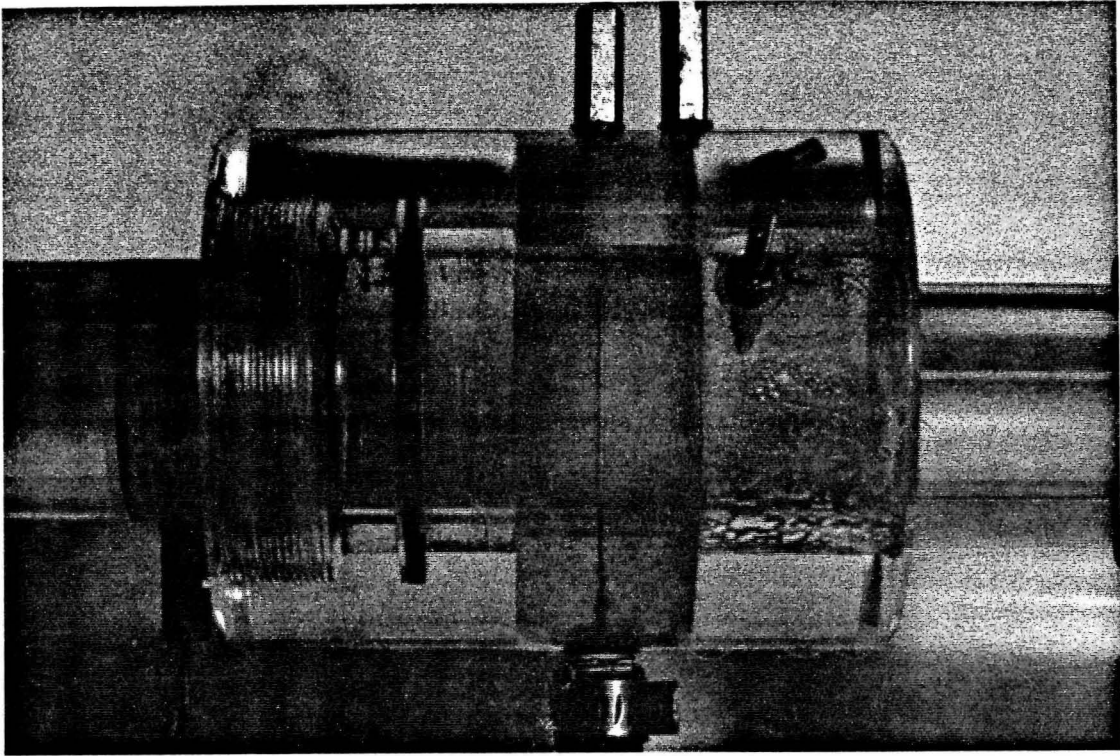
Figure 4.1: Flow visualization in test section at low pipe flow.

maintain a constant flow rate as the pipe flow rate varied.

4.3 Flow Visualization

To visualize the flow in the contraction and test section, red food coloring was introduced through a .5 mm hole 20 cm upstream of the contraction. The purpose was to see if any unpredicted flow patterns had developed and to determine if the flow in the pipe remained laminar. The flow field in the pipe appeared well behaved, smooth and without any swirling motion, although hints of turbulence were evident approximately 20 cm downstream of the slot at the highest velocities. At lower pipe flow rates and higher slot flows it was possible to see the dye enter the orifice chamber as shown in Fig. 4.1.

Chapter 5

Presentation of Data and Discussion

5.1 Data Reduction

The data were entered directly into a computer, electronic spreadsheet, where the following equations were used to compute values. The viscosity was taken from the relation

$$\nu = \{1.005 - .0112777(T - 68)\}10^{-6} .$$ (5.1)

This equation was derived from fitting a straight line to published values for ν (m^2/s) as a function of temperature in °F.

The pressure drop across the slot is given by

$$\Delta p = g\rho z ,$$ (5.2)

where z is the manometer reading.

The slot bulk velocity is

$$u_s = \frac{q_s}{2\pi rw} ,$$ (5.3)

while the pipe bulk velocity is

$$U_m = \frac{q_p}{A_p} = \frac{1.79f}{\pi r^2} = .2229f ,$$ (5.4)

where f is the frequency from the Flosensor in Hertz and U_m is in m/s.

The orifice discharge coefficient is defined as

$$C_d = \frac{\text{actual flow}}{\text{ideal flow}} = \frac{q_s}{A_s\sqrt{2\frac{\Delta p}{\rho}}} = \frac{1}{\sqrt{C_p}} \, , \qquad (5.5)$$

where

$$C_p = \frac{\Delta p}{\frac{1}{2}\rho u_s^2} \, . \qquad (5.6)$$

The error associated with these variables is indicated by the error bars in the figures. For a discussion concerning the accuracy of the results, see Appendix B.

5.2 Results for Zero Pipe Flow

The condition of zero pipe flow corresponds to the usual flow conditions for which discharge coefficients have been reported. The results for zero pipe flow are plotted in Fig. 5.1 along with the data of previous investigators. For comparison, a line was obtained from the following formula from Idel'Chik [9, Diagram 4-18, p. 174]:

$$C_p = C_{p\phi} + \varepsilon(\lambda + C_{po}) \, , \qquad (5.7)$$

where $C_{p\phi}$ and ε are functions of Re_w, while λ and C_{po} are functions of the geometry of the orifice. For a slot $\lambda = 96/Re_w$, while for an aspect ratio (h/w) of 4, $C_{po} = 1.55$. The values for $C_{p\phi}$ and ε are taken from curves obtained empirically by Idel'Chik.

The x data points in Fig. 5.1 are from similar work by A.S.W. Thomas and K.C. Cornelius [16] for $h/w = 6.6$. The rest of the data points are from the present investigation for various slot sizes 0.13 mm, 0.24 mm, and 0.5 mm, which correspond to aspect ratios of 24, 13, and 6.4, respectively.

Some general trends emerge: At low Re_w the discharge coefficient is low, but tends towards the potential flow prediction of unity as Re_w increases. Also, the

smaller the slot width, the lower the C_d. Idel'Chik's formula fits these data best between Re_w less than 500 and greater than 200. Furthermore, Idel'Chik's results show a good fit of the Thomas and Cornelius data, both of which are for a flat-plate flow field. An explanation for the differences between the present data and the results from others can only be conjectured. Perhaps the different geometry, uncertainties about the exact width of the present slot, or the high aspect ratios (h/w) involved in this experiment are responsible.
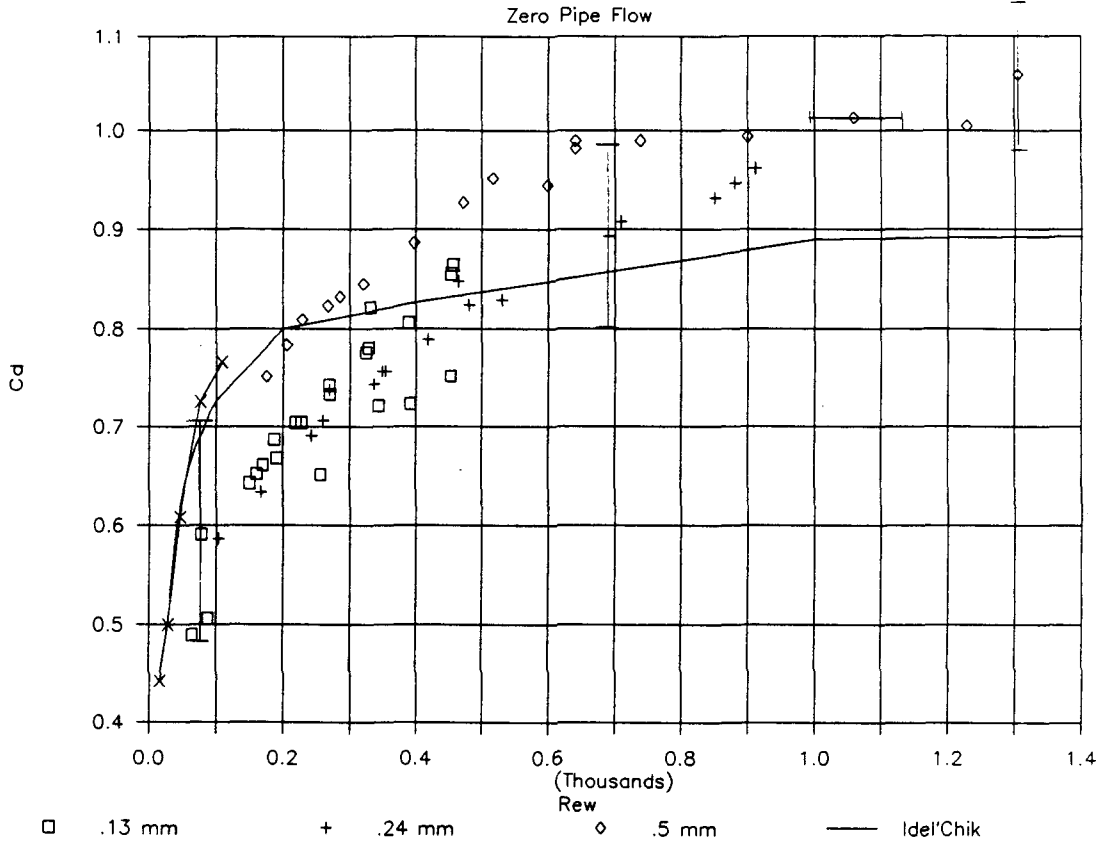
Figure 5.1: Orifice coefficients for zero pipe flow. The line is from Idel'Chik [9], while the × data points are from A.S.W. Thomas and K.C. Cornelius [16].

5.3 Results with Pipe Flow

This section addresses the main subject of this investigation, which is to determine the effect of a passing freestream velocity on flow through a slot.

5.3.1 Discharge Coefficient versus Slot Reynolds Number

The most direct manner to present the data is plotted in Figs. 5.2, 5.3, and 5.4, which show how C_d varies with Re_w for various U. Each figure is for a given slot width, while the different symbols represent the various pipe velocities in meters per second. The line in Fig. 5.2 is a best-fit curve of the zero pipe flow data.

The shape of the several curves is similar, in most cases, to that of the zero flow case. In other words, a low slot-flow rate implies low C_d, which increases as with Re_w. For some of the flows, however, we see a maximum C_d.
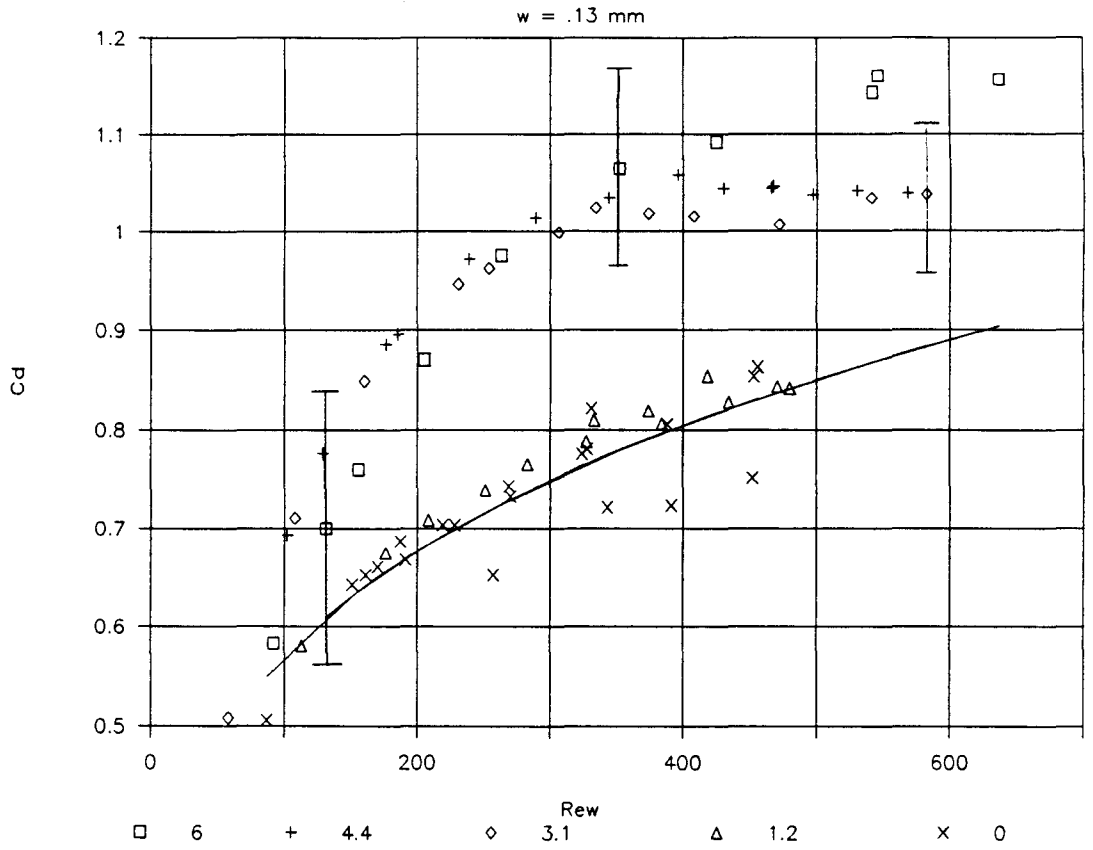
Figure 5.2: Comparison of C_d to Re_w for $w = .13$ mm.
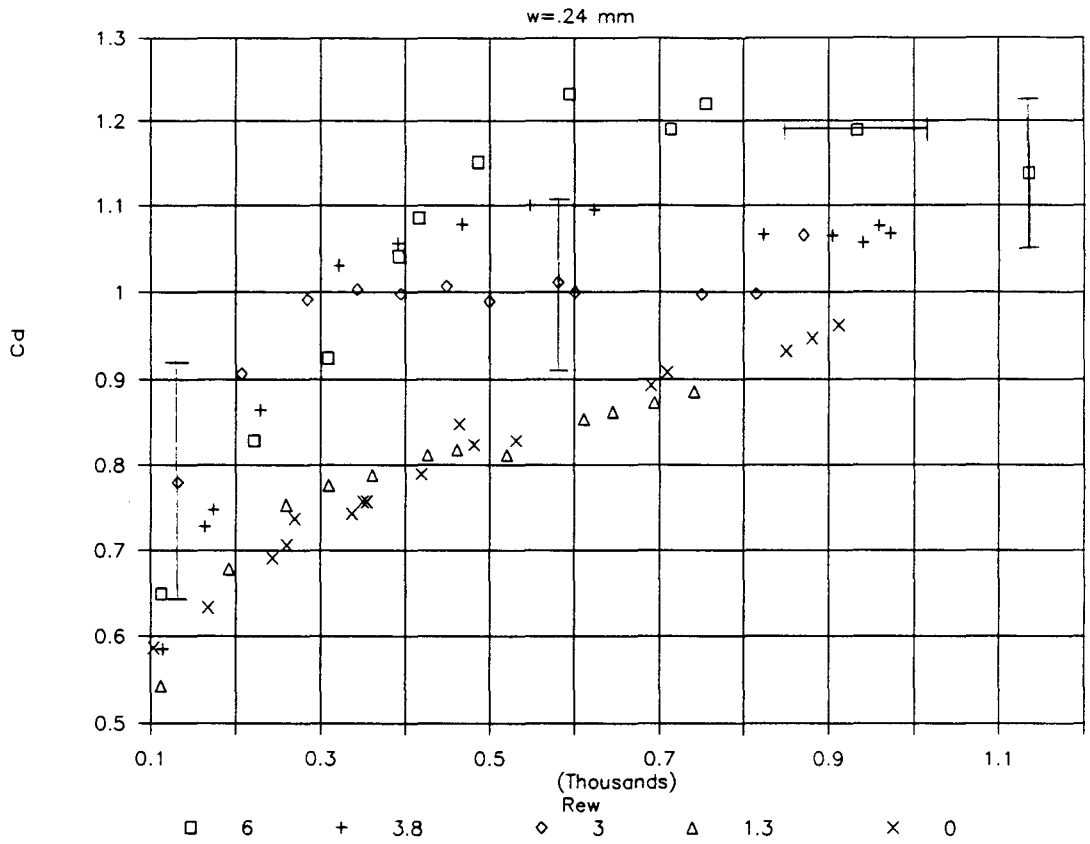
Figure 5.3: Comparison of C_d to Re_w for $w = .24$ mm.
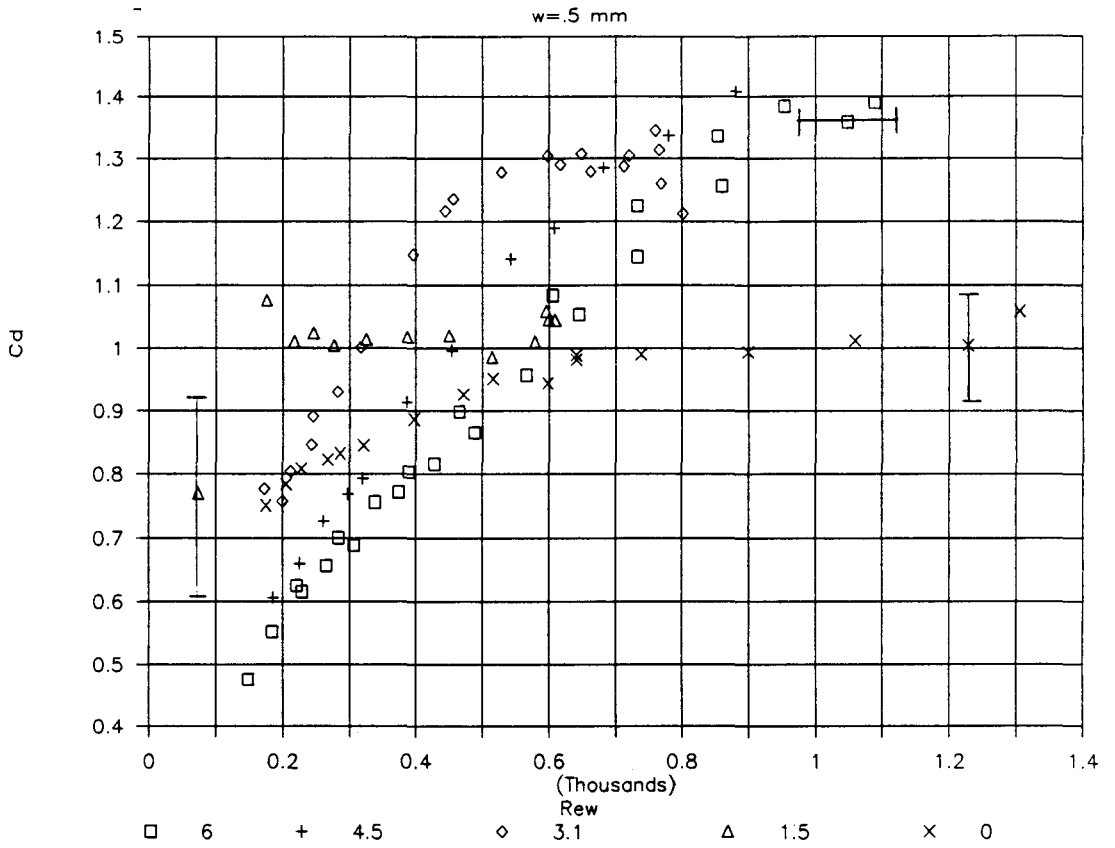
Figure 5.4: Comparison of C_d to Re_w for $w = .5$ mm.

5.3.2 Discharge Coefficient Difference

To emphasize the difference between C_d for a zero pipe-flow situation and C_d when there is a passing flow, another variable, ΔC_d, is defined as follows:

$$\Delta C_d = C_d - C_{do} , \qquad (5.8)$$

where C_{do} is C_d at zero pipe flow. In order to determine ΔC_d, a regression was performed on the no-flow data points (C_{do}). Various types of curve-fitting techniques were tried. For all three slot widths, the best-fit equation for C_{do} was of the form

$$C_{do} = B Re_w^K , \qquad (5.9)$$

where B and K are constants. The values for B and K are given in Figs. 5.5, 5.6, and 5.7.

Some observations: With the small slot width, any pipe flow will increase ΔC_d to some extent, whereas for the larger slot there is a region of low Re_w and high pipe flow, where the ΔC_d is negative. Furthermore, the data for the small slot show a clear maximum for ΔC_d as a function of Re_w, while for the larger slot width, this maximum is not always present, especially at the higher pipe flows.

One possible explanation for this behavior is that the characteristics of the separation bubble in the slot have an effect on the flow. Thomas and Cornelius [16] studied this bubble in detail (see Fig.1.1). One of their results included a method of predicting the reattachment point of the separation bubble based solely on values of α and Re_w. The dimensionless velocity gradient (α) is defined as follows:

$$\alpha = (du/dy)(w/u_s) . \qquad (5.10)$$

The length of the separation bubble (b) is given by:

$$b = \frac{w Re_w^{3/4}}{7.5} \tan^{-1}(\frac{\alpha}{2.5}) . \qquad (5.11)$$

From this equation, one would predict that in the 0.5 mm slot, the separation bubble does not reattach for all except the slowest flow of 1.5 m/s. For the two smaller slots, however, the bubble always reattaches. Therefore, one might speculate that when the bubble reattaches, the curves show a clear maximum (see Figs. 5.5 and 5.6), but that when the bubble fails to reattach, the curves are nearly linear and have negative values at low Re_w (see Fig. 5.7). The only exception to this trend is the 3.1 m/s flow rate in Fig. 5.7, for which reattachment is not predicted yet a maximum in C_d exist. Whether or not the behavior of the separation bubble is the proper explanation of the nature of the data in Figs. 5.5, 5.6 and 5.7 is, of course, purely conjecture at this time.

These plots also show that ΔC_d is unaffected by low pipe velocities for the small slot widths. In addition, for the 0.5 mm slot width ΔC_d not only is increased by the small, freestream velocity, but is 50% better than the ΔC_d at the same Re_w for the high speed pipe flow. Furthermore, the curve of the data at the 1.5 m/s pipe velocity is significantly different than that in the 6 m/s case.
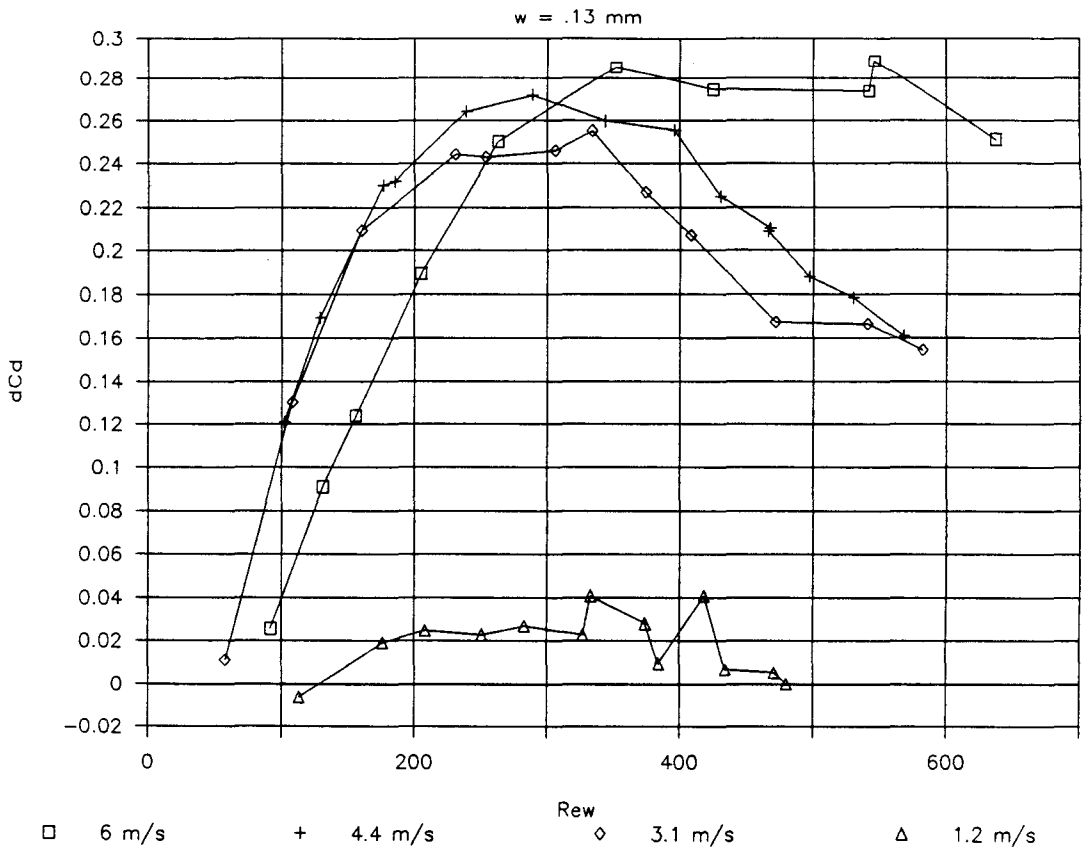
$A = .18$ and $B = .25$

Figure 5.5: Comparison of ΔC_d to Re_w for $w = .13$ mm.
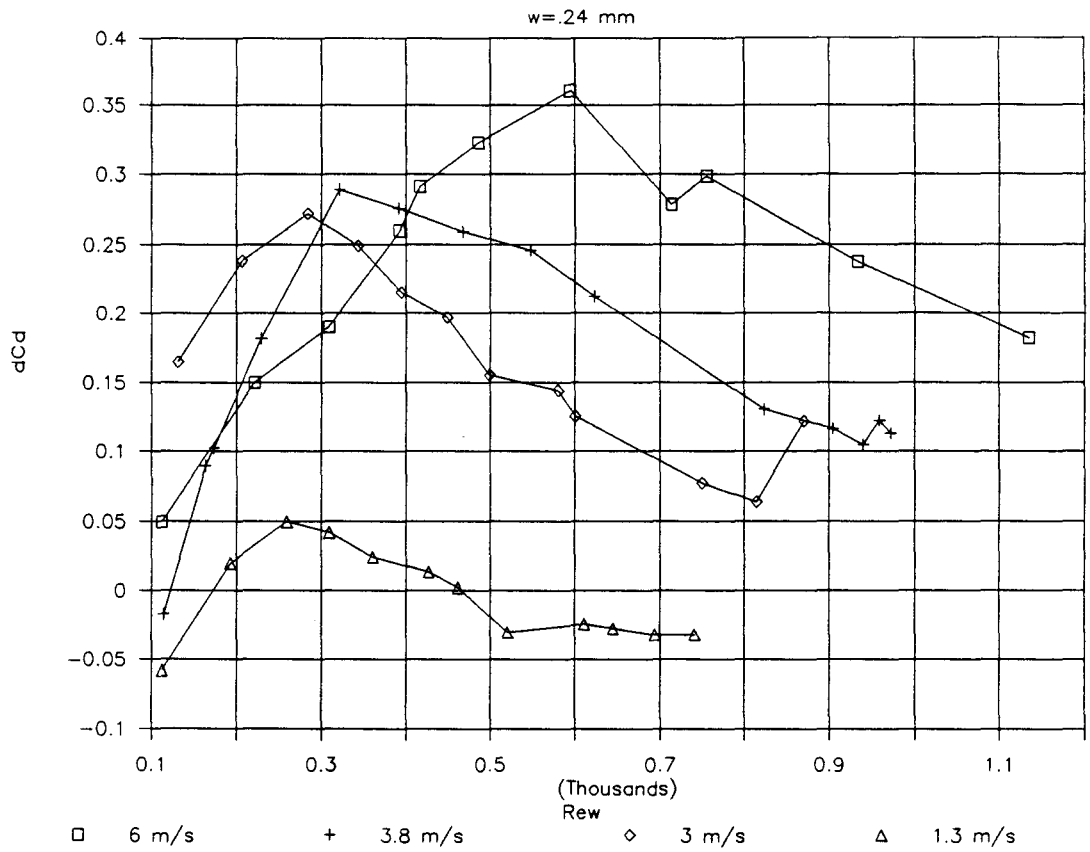
$A = .2$ and $B = .23$

Figure 5.6: Comparison of ΔC_d to Re_w for $w = .24$ mm.
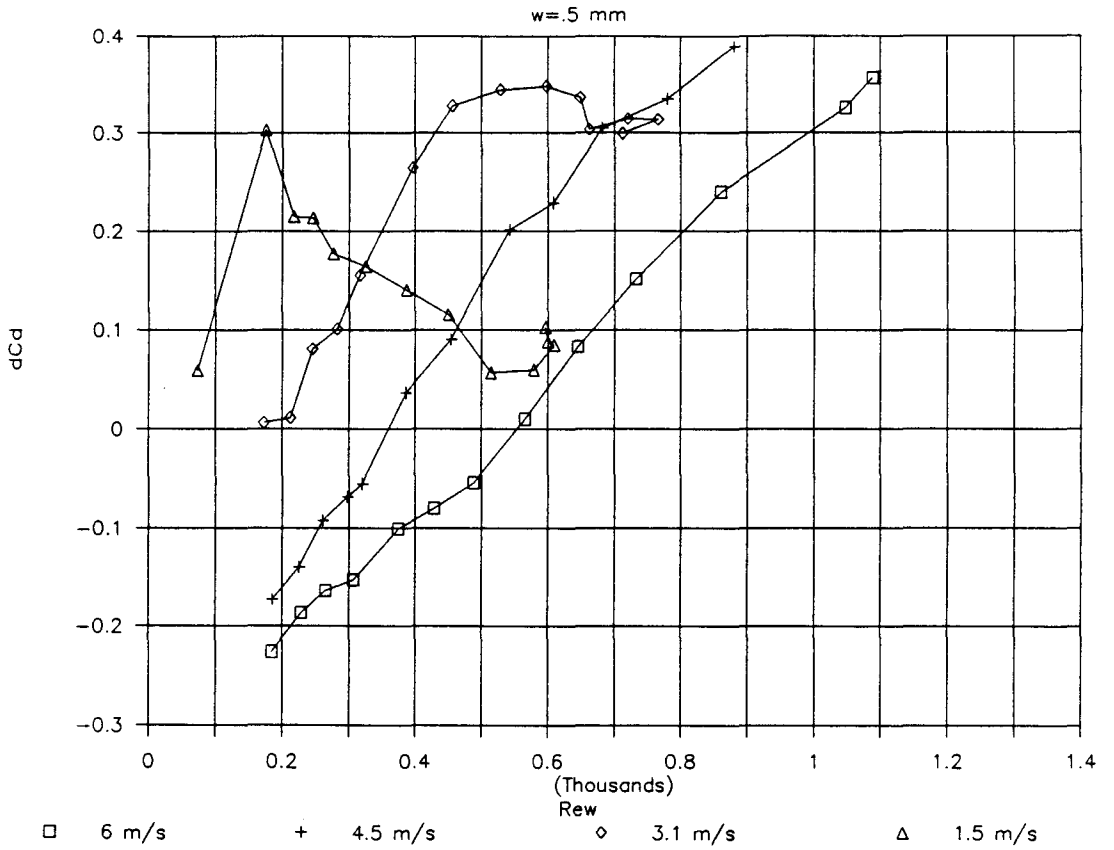
w=.5 mm

$A = .34$ and $B = .16$

Figure 5.7: Comparison of ΔC_d to Re_w for $w = .5$ mm.

5.3.3 Discharge Coefficient versus Pipe Velocity

This method of representing the data involves using the results of data taken with constant slot flow as described in Section 4.2. These results are plotted in Figs. 5.8, 5.9, and 5.10. Additionally, the plots also show data taken with constant pipe flow interpolated mathematically to conform to the present form of representation. This was accomplished by curve-fitting all the data taken with constant pipe flow to an equation of the form

$$C_d = A + B Re_w + C Re_w^2 + D Re_w^3 . \qquad (5.12)$$

The value of Re_w would then be held constant and different points plotted for the various values of Re_x. In the figures, these cross-plotted results are represented by the symbols connected by lines, while the unconnected symbols represent actual data points for various Re_w taken with a constant flow in the slot.

As with the previous plots, there are some trends that are highly dependent on the slot width or perhaps more generally on the aspect ratio ($\frac{h}{w}$). These differing trends are most evident for the narrowest and widest slot width, but are not nearly as clear for the .24 mm slot width. For the smallest slot width there is a trend for C_d to increase with U for $Re_w > 200$. However, for the largest slot width, C_d increases with U initially, then decreases with increasing U. Furthermore, it is evident for the narrow slot that a small pipe velocity will cause no change or decrease C_d, while the opposite is true of the wider slot width. The .24 mm slot seems the show traits of both the other two.

As a general observation, C_d varies with the velocity in the pipe and a maximum C_d occurs at some nonzero pipe flow. This maximum was noted by Thomas, Cornelius [16] and Khanzhonkov [10]. Apparently, at certain pipe velocities the av-
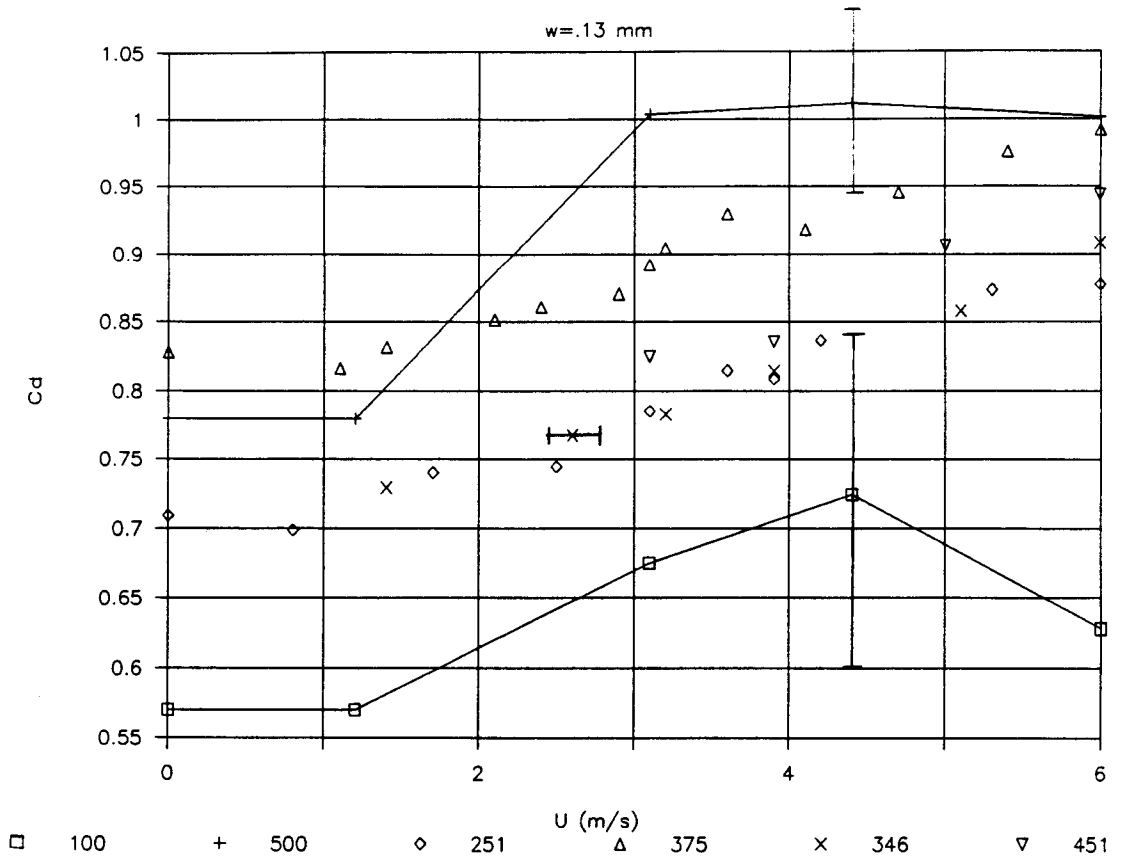
Figure 5.8: Comparison of C_d to Re_x for $w = .13$ mm.

erage momentum in the flow aids the flow into the slot. As the freestream velocity increases, thus increasing dU/dy, the suction flow comes from a region closer to the wall. Thomas and Cornelius [16, page. 795] have suggested that this high shear flow must turn more sharply as it enters the slot and thus incurs more losses than a slower flow. This theory seems to explain the maximum in C_d as a function of U when it occurs.
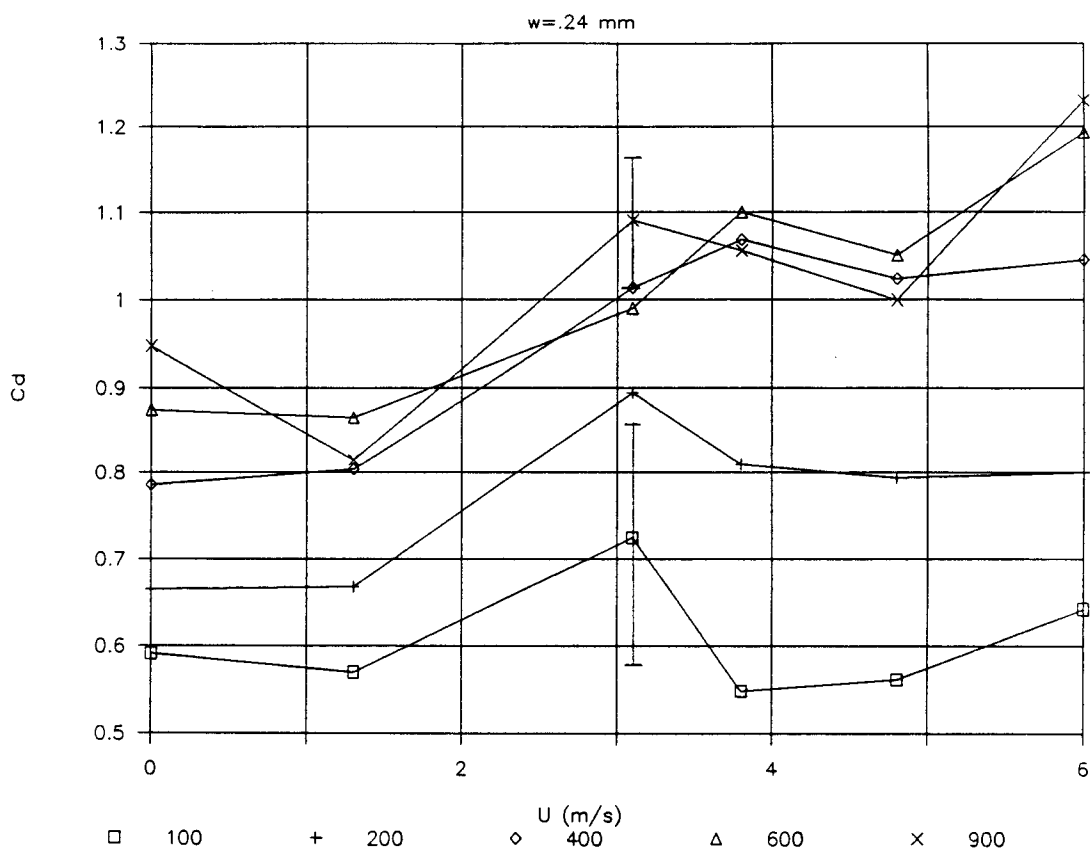
Figure 5.9: Comparison of C_d to Re_x for $w = .24$ mm.
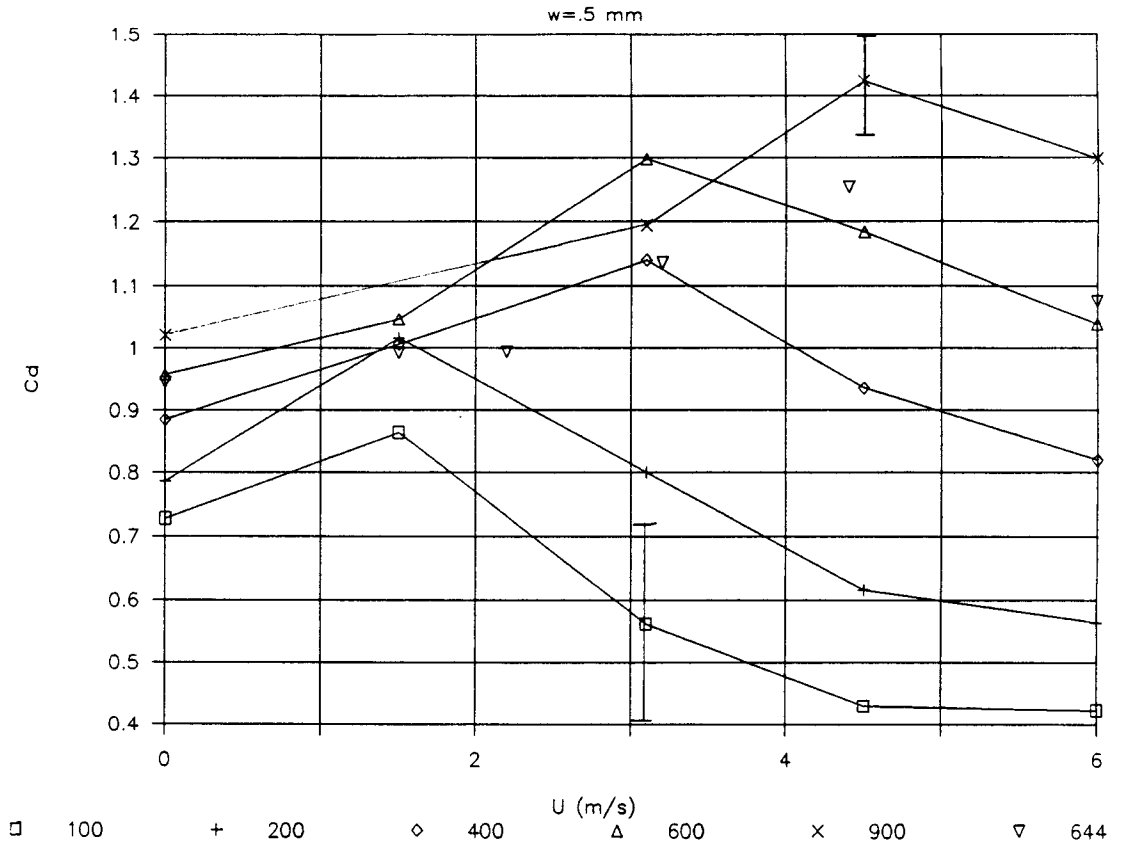
Figure 5.10: Comparison of C_d to Re_x for $w = .5$ mm.

5.3.4 Discharge Coefficient versus Velocity Ratio

Khanzhonkov [10] relates C_d to the velocity ratio (U/u_s) as is done in Figs. 5.11, 5.12, and 5.13. For comparison, results from Khanzhonkov are shown by the line in Fig. 5.13 . His experiments included both circular and rectangular orifices, both of which probably had very small aspect ratios. The results, obtained by Khanzhonkov, are valid only for $Re_w > 10^4$, and the flow field was probably such that the separation bubble was detached. In this regime, the assumption that U/u_s is the most significant parameter may well be justified. In comparing the results by Khanzhonkov to the present, the differences in flow conditions and Re_w have to be kept in mind, since they may explain at least some of the differences in the numerical values for C_d.

As before, the significant trends are highly dependent on the aspect ratio. The two narrower slots have separate curves for each pipe flow, while most of the data points for the wide slot fall on a single curve. In the widest slot, the 1.5 m/s velocity data show the greatest deviation from the single curve. Interestingly, this is also the only pipe velocity in the 0.5 mm group where the bubble reattaches itself. The bubble characteristics were inferred from the results of Thomas and Cornelius [16] outlined in Sec. 5.3.2. These plots offer the clearest indication that there is a strong correlation between the reattachment of the separation bubble and C_d, since only the flows without reattachment fall onto the single curve shown in Fig. 5.13. Generally, the maximum C_d for $U > 2$ m/s occurs when $1 < U/u_s < 3$.
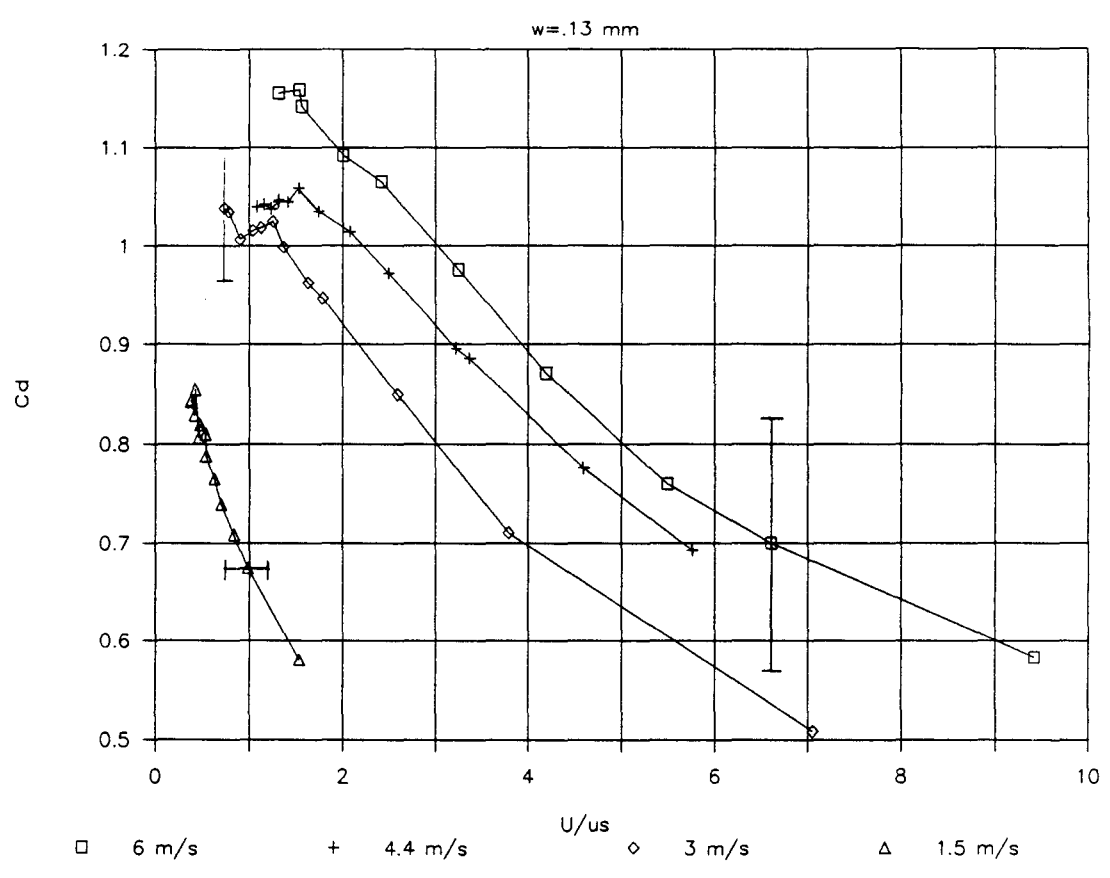
Figure 5.11: Comparison of C_d to (U/u_s) for $w = .13$ mm.
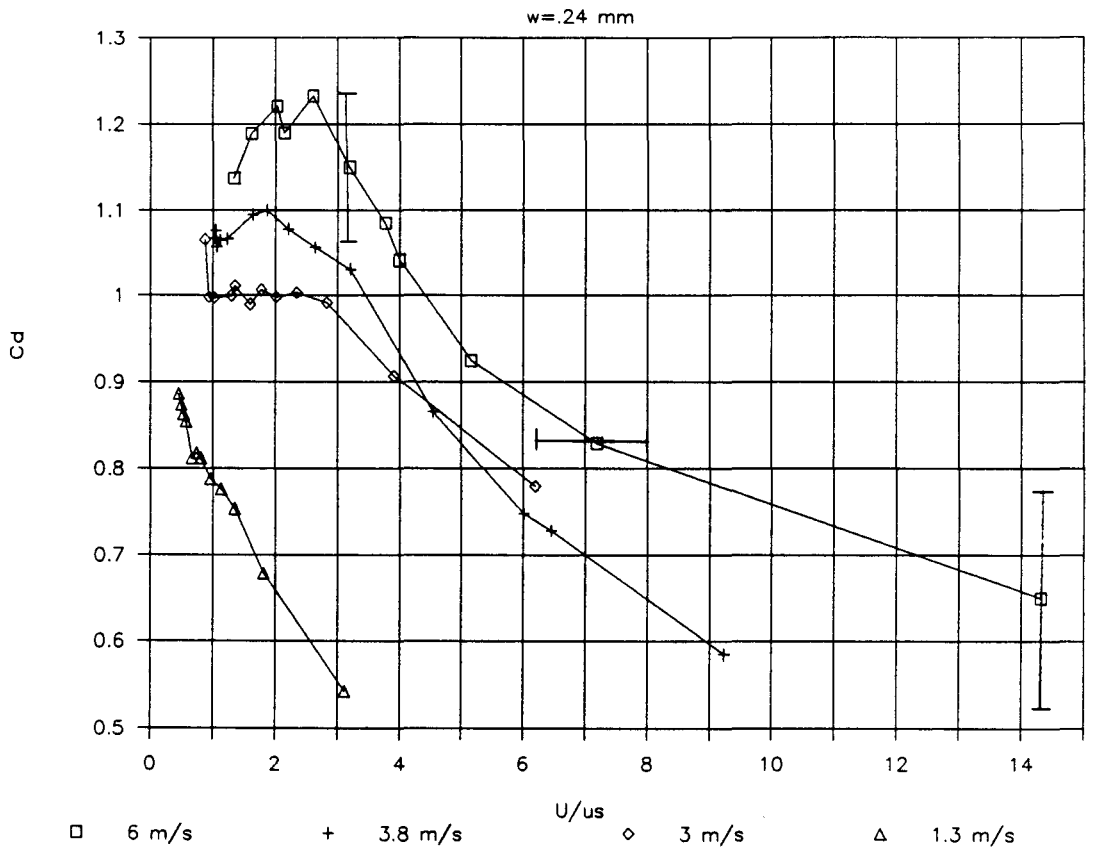
Figure 5.12: Comparison of C_d to (U/u_s) for $w = .24$ mm.
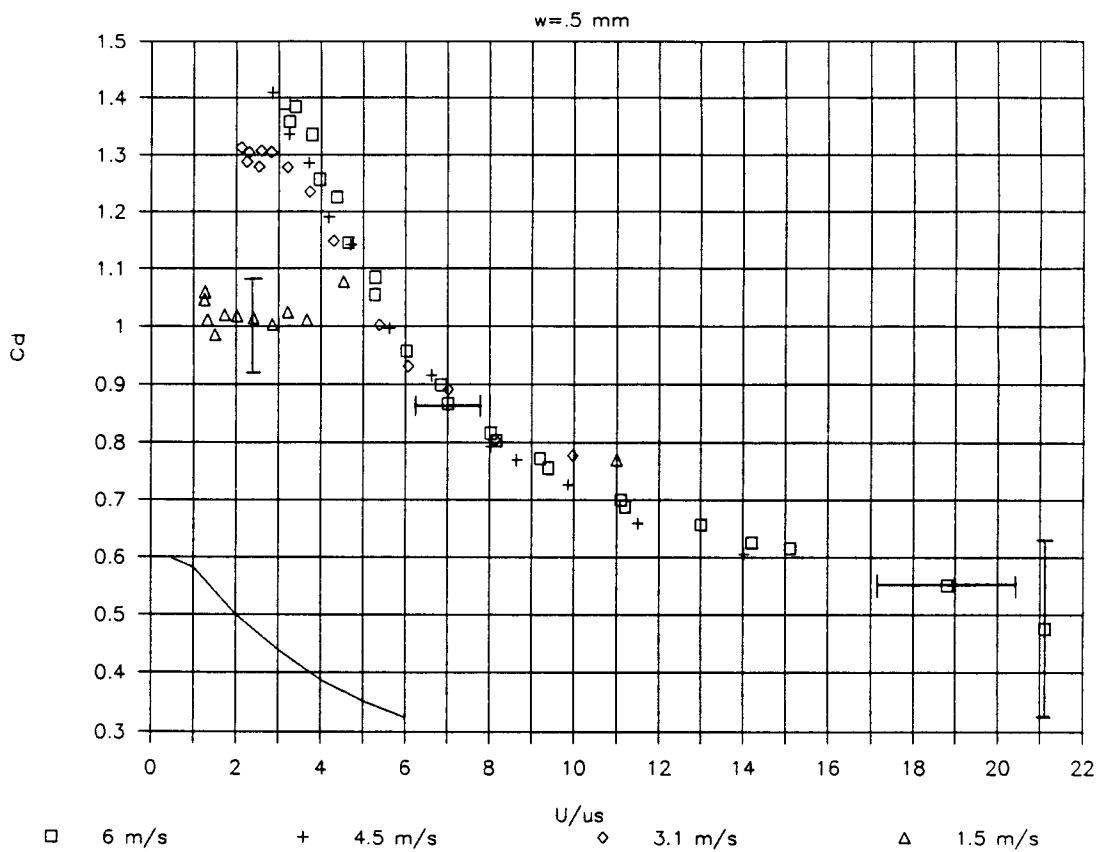
Figure 5.13: Comparison of C_d to (U/u_s) for $w = .5$ mm.

5.3.5   Freestream Dynamic Head Recovery versus Velocity Ratio

To interpret the results, another coefficient may be formulated that gives the percentage of the freestream flow recovered by the slot, which is defined as follows:

$$S_a = \frac{\text{Virtual dynamic head recovered}}{\text{Actual freestream dynamic head}} = \frac{\Delta p^*}{\frac{1}{2}\rho U^2} , \qquad (5.13)$$

where Δp^* is defined by the relation

$$C_{po} - C_p = \frac{\Delta p^*}{\frac{1}{2}\rho u_s^2} . \qquad (5.14)$$

By rearranging Eqns. 5.13 and 5.14, the following result is achieved:

$$S_a = (C_{po} - C_p)(\frac{u_s}{U})^2 . \qquad (5.15)$$

An equivalent and perhaps clearer way to write S_a is as follows:

$$S_a = \frac{p_o(U) - p_o(0)}{\frac{1}{2}\rho U^2} , \qquad (5.16)$$

where $p_o(U)$ and $p_o(0)$ are the static pressures in the orifice chamber (see Fig. 2.4), with and without pipe flow, respectively.

Figs. 5.14, 5.15, 5.16 and 5.17 compare S_a to the velocity ratio. Interestingly, for $U > 2$ m/s, all the data, with some scatter, fall onto a single hyperbolic curve. This curve is asymptotic, as $u_s \to 0$ along the horizontal axis $S_a \to 0$. This situation is analogous to little or no flow in the slot; therefore, no pressure recovery. The slot is simulating a pressure tap. On the other extreme, as $U \to 0$, $S_a \to \pm\infty$, since virtually all of the small, freestream dynamic head is recovered. However, when $U = 0$, S_a is undefined. A best-fit equation for this hyperbolic curve, which is represented by the line in Fig. 5.16, is given by:

$$S_a = .15 - .116 \ln(U/u_s) - .021[\ln(U/u_s)]^2 . \qquad (5.17)$$

Fig. 5.17 includes data from all three slot sizes, but does not include data for $U < 2$ m/s. For reasons not completely understood, the low pipe-velocity flows do not conform to the curve as well as the higher velocity flows and are not shown in Fig. 5.17, but are given in Fig. 5.18. One cause of the difference in the slower velocity data is the high experimental error associated with U as it approaches zero, which is discussed in Appendix B. Furthermore, there is little difference between C_{po} and C_p at the lower pipe-flow rates and narrower slot sizes.
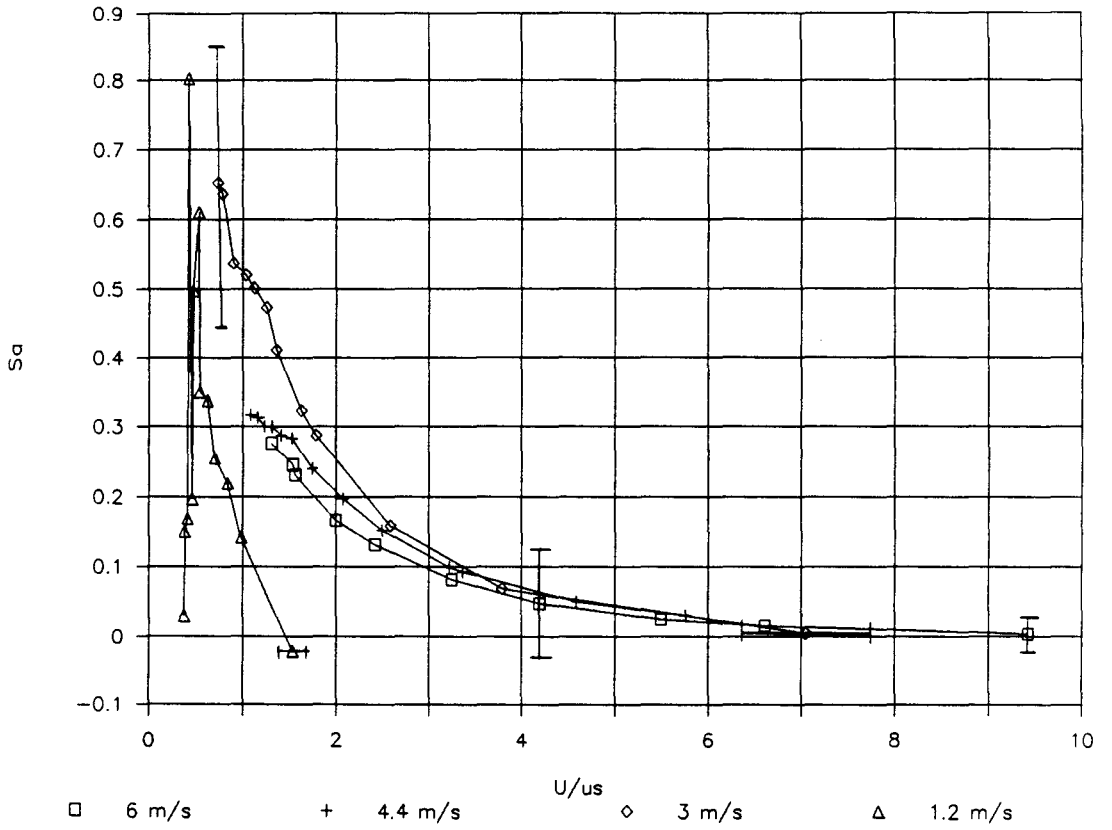
Figure 5.14: S_a versus the velocity ratio for w=.13 mm.
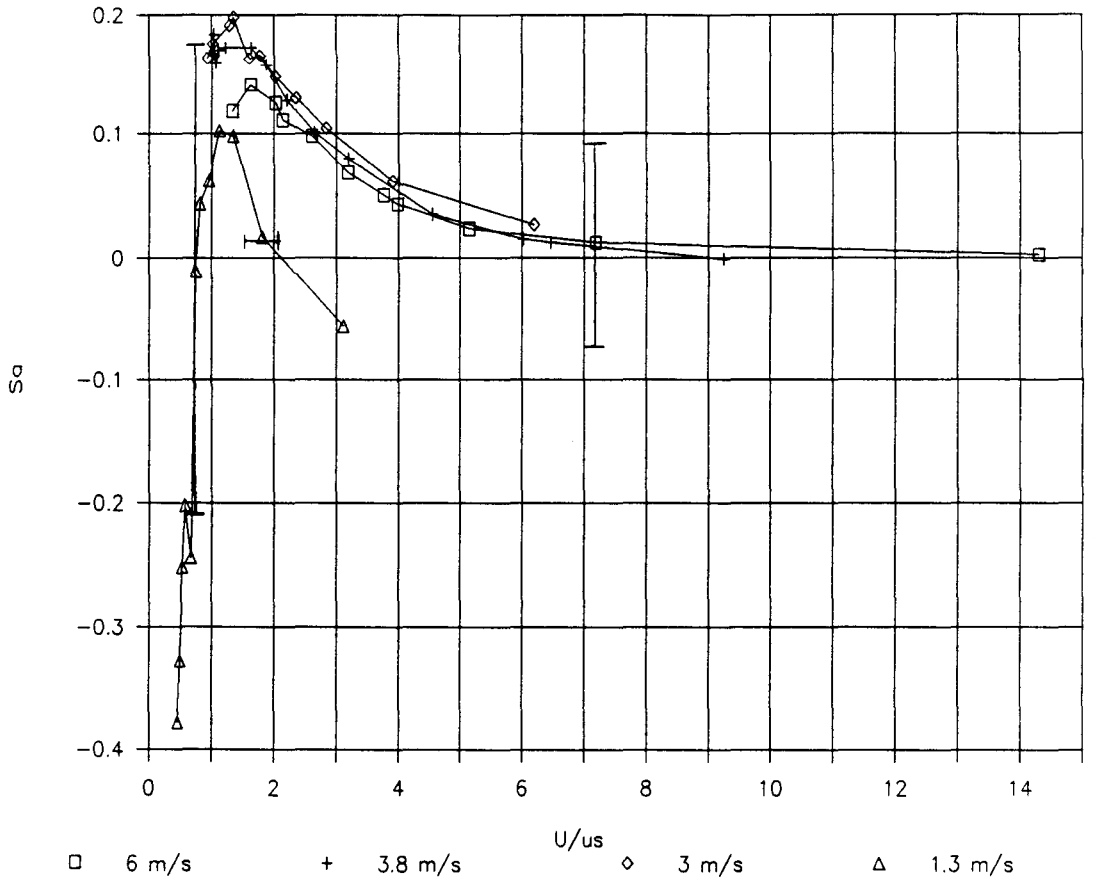
Figure 5.15: S_a versus the velocity ratio for w=.24 mm.
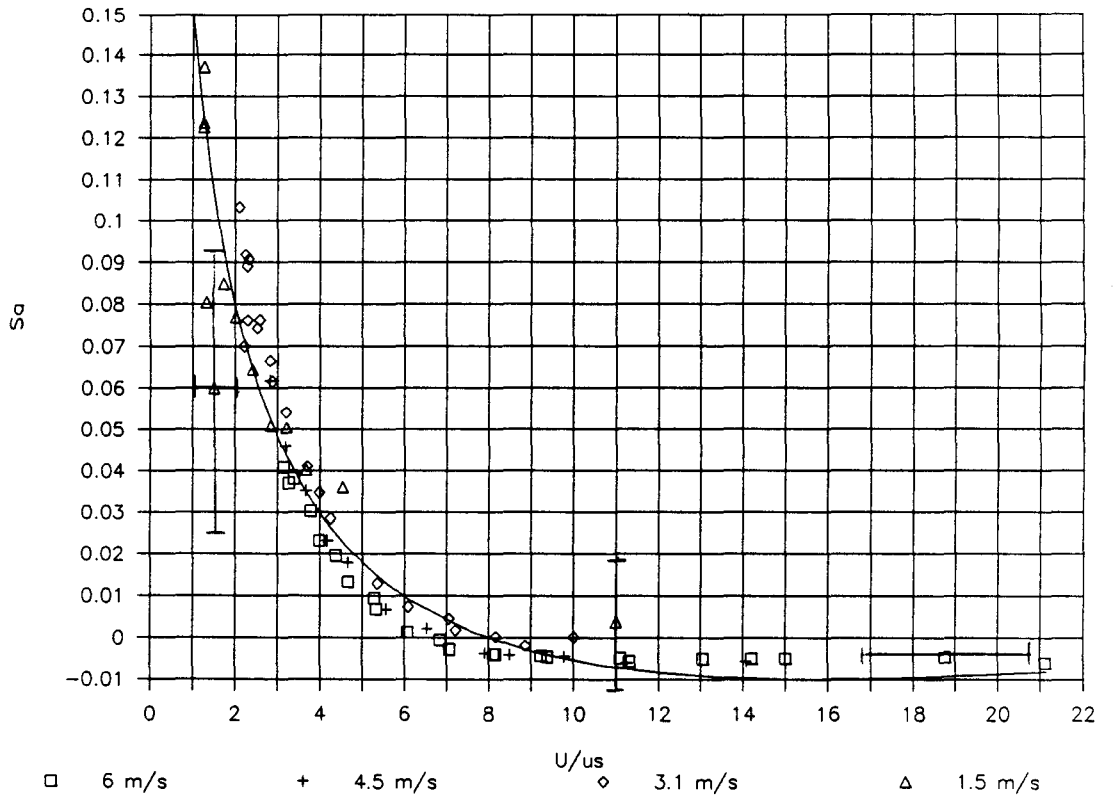
Figure 5.16: S_a versus the velocity ratio for w=.5 mm.
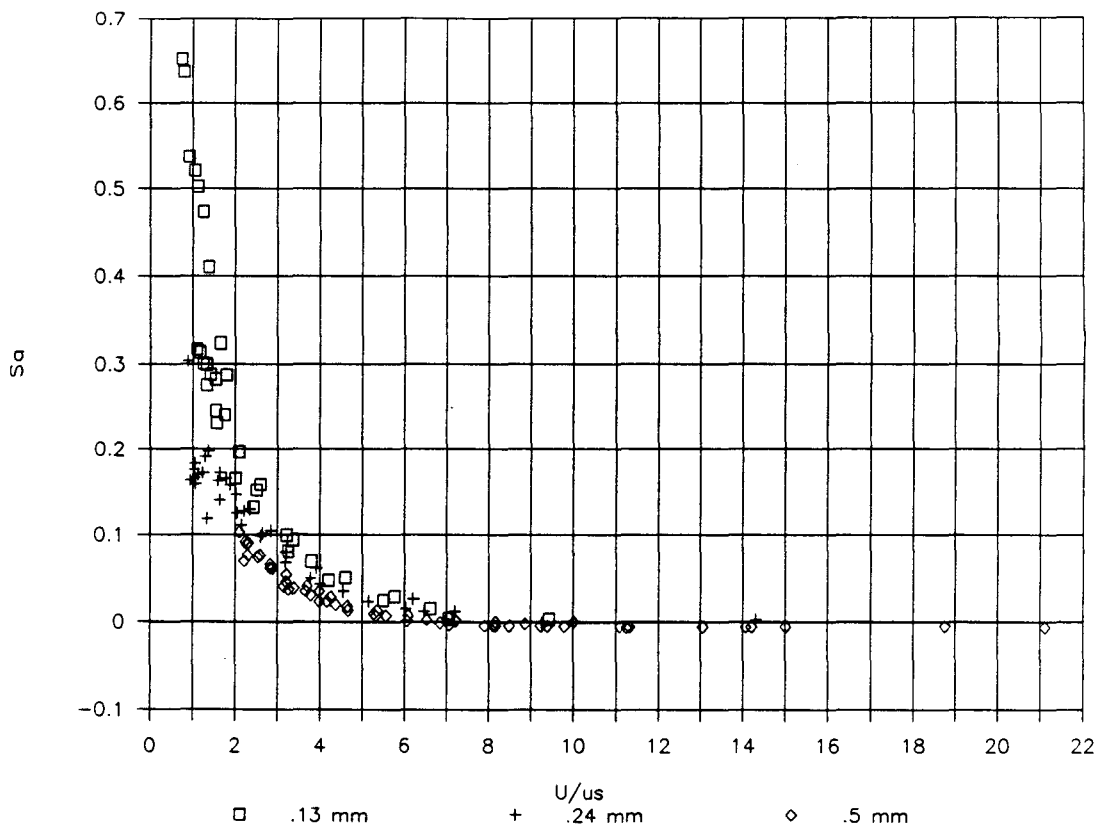
Figure 5.17: S_a versus the velocity ratio, $U > 2$ m/s.
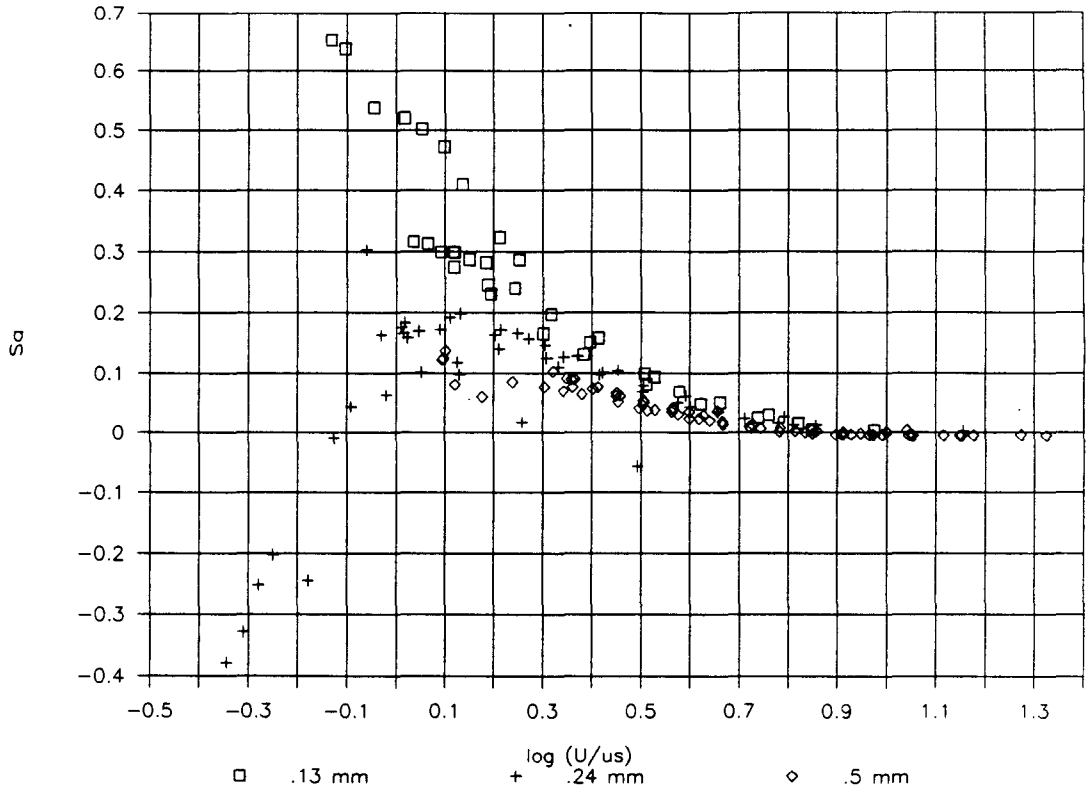
Figure 5.18: S_a versus the logarithm of the velocity ratio.

5.3.6 3-Dimensional Representation

Figs. 5.19, 5.20, and 5.21 were made from a 3-dimensional plotting program called "SURFER" [19]. Unlike the previous graphs where only the most recent data points are plotted, these plots include all of the data available. The program fits a mesh to the data, in this case using the Kriging Method, and then smooths the results mathematically.

The 3D plots provide an interesting perspective to the data while illuminating and accentuating differences in the data for the different sized slots. In terms of general trends, the .13 mm plot shows C_d increasing as either Re_w or Re_x rise. The small hills and valleys are caused mainly by variance in the data, not by an actual phenomenon. The experimental error was greatest for the narrow gap, and some of this deviation in the data appears in this plot.

The .24 mm gap profile is much smoother and shows its trends more clearly. Again, we find C_d increasing with Re_w, but its relationship with Re_x is not as clear, whereas, the .5 mm gap surface shows some roughness from discrepancies in the data and a ridge of maximum C_d.
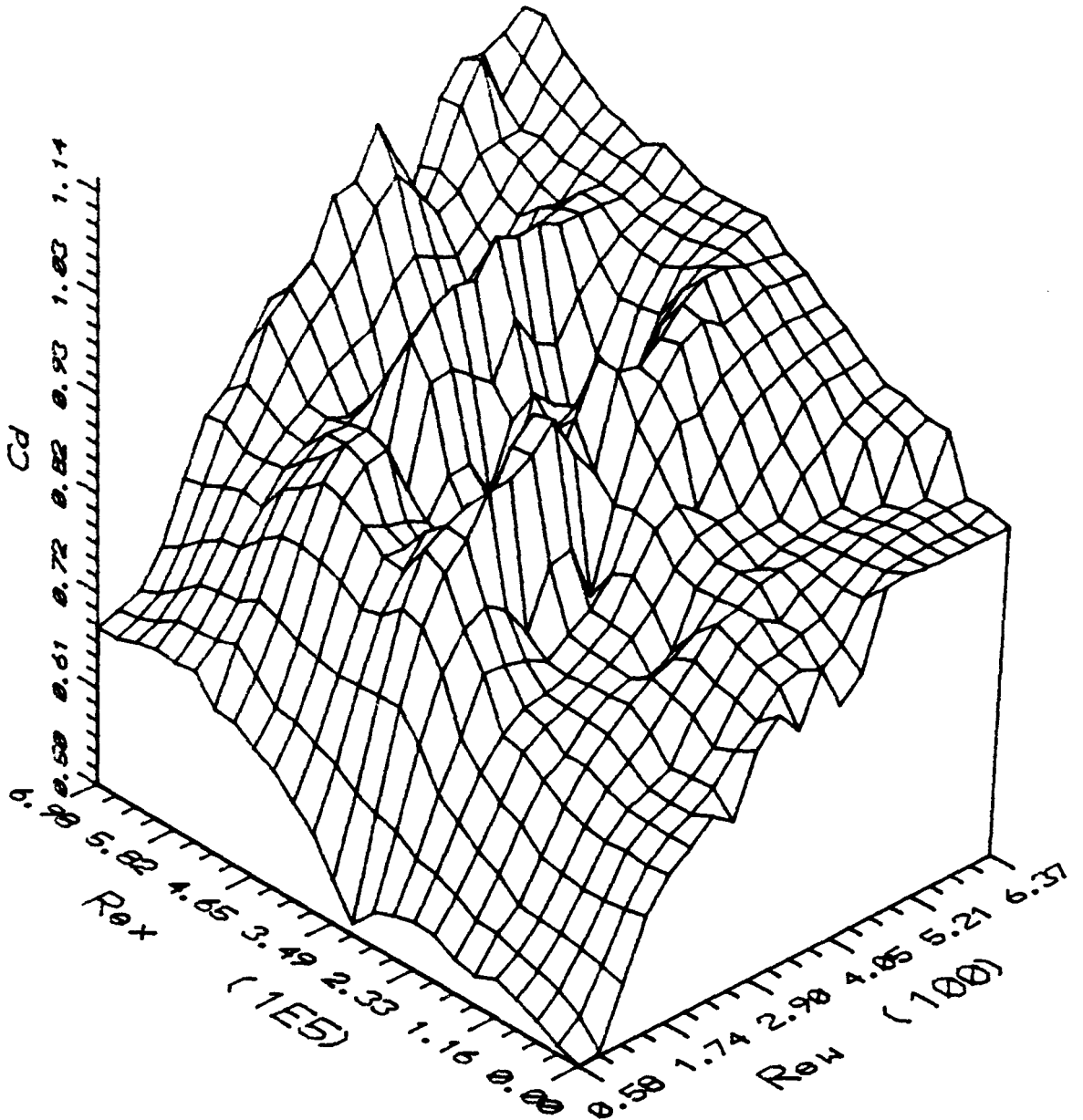
Figure 5.19: A 3D view for w=.13 mm.
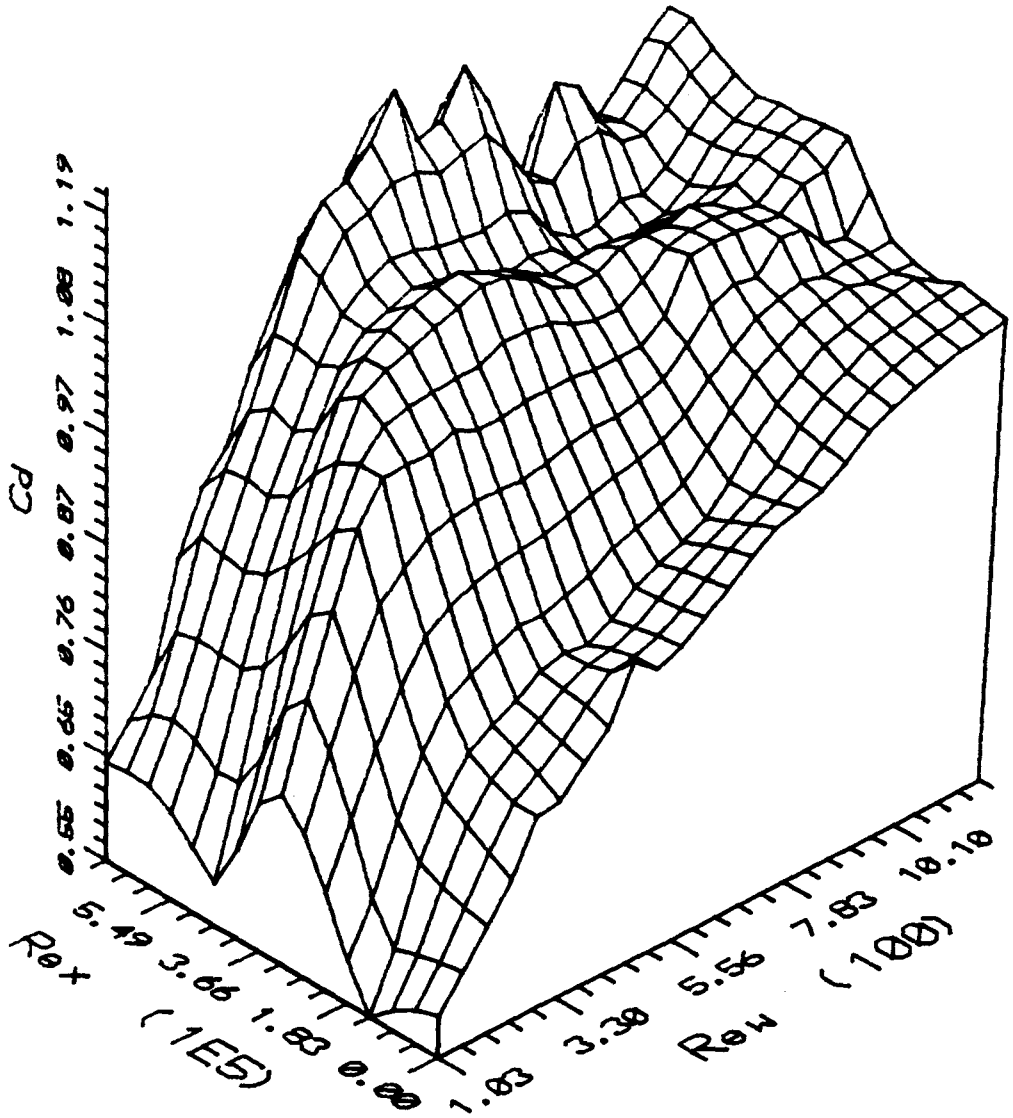
Figure 5.20: A 3D view for w=.24 mm.
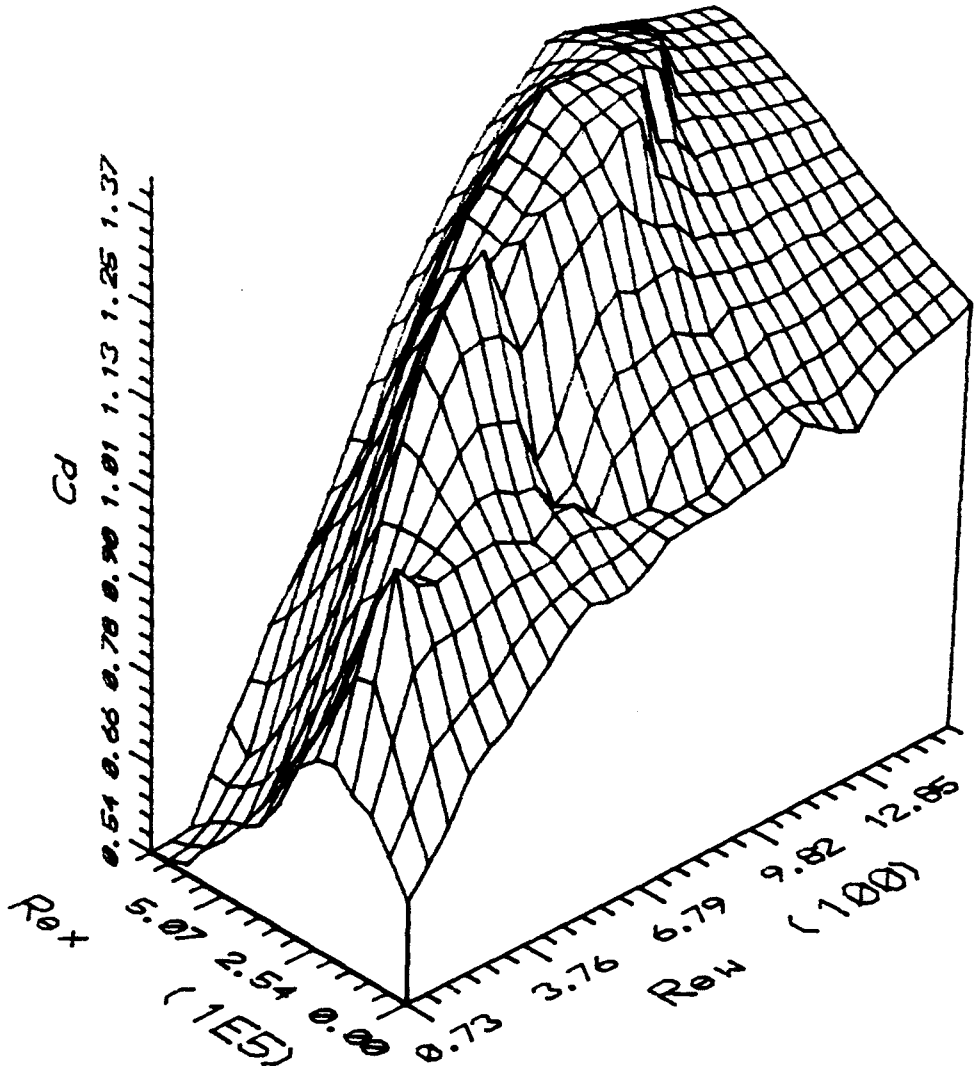
Figure 5.21: A 3D view for w=.5 mm.

Chapter 6

Summary and Conclusion

As stated in the introduction, the general purpose of the present project was to assess the effect of a flow along a wall on the discharge coefficient for an orifice or slot in this wall. In particular, it was to be determined if the velocity head of the freestream flow would tend to increase the flow through the slot. The problem may be well illustrated by an example. Assume that under certain conditions the static pressure difference across the slot is 0.1 m of water. In the absence of any velocity along the wall, this pressure difference would be the driving force determining the flow rate through the slot. Next, let us raise the freestream velocity to 6 m/s and maintain the same static pressure difference. The dynamic head upstream of the slot is now about 1.8¿m. If the full dynamic head were recovered, the flow through the orifice would be expected to increase according to the approximation

$$\frac{u_s}{u_{s_o}} = \sqrt{1 + \frac{\frac{1}{2}\rho U^2}{\Delta p_o}} \, . \tag{6.1}$$

For the example, $(u_s/u_{s_o}) \approx 4$. The fact that the stream entering the slot comes from a layer near the wall, which moves at lower velocities will reduce this factor, but the effect would still be a major one. When surveying the full set of data, no major effect of this kind was noted. The largest increase in the discharge coefficient that was recorded occurred when the velocity along the wall was 4.5 m/s, and the static

pressure difference was .064 m. The discharge coefficient under these conditions was 1.41, and the corresponding discharge coefficient without any freestream velocity was .98 . If the entire increase in the coefficient was attributed to recovery of the freestream dynamic head, then this increase would correspond to only a 6.2% recovery of the dynamic head. It may be concluded, therefore, that for the present geometry and for the rather wide range of variables that have been investigated, the recovery of the freestream dynamic head does not lead to any major increases in the flow through slots. Major increases, in this context, are defined as changes that would reflect full recovery of the freestream dynamic head.

Nevertheless, the effect of the approaching flow on the slot discharge coefficient is certainly not negligible. Values for ΔC_d $(C_d - C_{do})$ were observed between $+0.4$ and -0.2. The exact magnitude will depend on the slot Reynolds number (Re_w), the velocity ratio (U/u_s), the character of the mainstream boundary-layer, as well as the slot geometry. Some of these effects were investigated in the present study, from which come the following conclusions:

1) For flows where the separation bubble reattachment is not predicted, C_d appears to be a function of only the velocity ratio and, perhaps, the slot geometry.

2) The freestream dynamic head recovery coefficient (S_a) has been measured for three slot sizes. Apparently, if U is greater than approximately 2 m/s, then as the velocity ratio increases, S_a becomes a strong function of U/u_s and loses its dependency on the slot width.

3) There are many variables involved in the slot-flow problem. Because of this, further work will be needed to establish relationships that may be used with confidence in predicting the discharge coefficient.

References

[1] Barker, S.J., and D. Gile 1981. Experiments on heat-stabilized laminar boundary layers in water. Journal of Fluid Mechanics 104: 139-158.

[2] Brandeis, J. 1983. Influence of Finite Slot Size on Boundary Layer with Suction or Injection. AIAA Journal 21 (4): 636-637.

[3] Chang, P.K. 1976. Control of Flow Separation New York: McGraw-Hill Book Company.

[4] Chmielewski, G.E. 1974. Boundary-Layer Considerations in the Design of Aerodynamic Contractions. Journal of Aircraft 11: 435-438.

[5] Goldsmith, J. 1956. Comparison of Calculated and Measured Laminar Suction Losses Through Small Round Holes with Sharp Edged Inlets. Northrop Aircraft. Norair Div. NAI-56-1110.

[6] Goldstein, S., ed. 1965. Modern Developments in Fluid Mechanics New York: Dover Publications, Inc.

[7] Gregory, N. 1961. Boundary Layer and Flow Control. Edited by G.V. Lachman, Vol. 2, Research on Suction Surfaces for Laminar Flow. New York: Pergamon Press.

[8] Hoerner, S. F. 1958. Fluid-Dynamic Drag Midland Park, New Jersey: By the author, 148 Busteed Drive.

[9] Idel'Chik, I.E., 1986, <u>Handbook of Hydraulic Resistance</u> New York: Hemisphere Publishing Corporation.

[10] Khanzhonkov, V.I. 1959. Resistance to the discharge through an orifice in the wall in the presence of the passing stream. <u>Prom. Aerodin.</u> (Oborongiz, Moscow) 15: 5-19.

[11] Lachmann, G.V., ed. 1961. <u>Boundary Layer and Flow Control</u> Vo.1 2. New York: Pergamon Press.

[12] Loehrke, R.I., and H.M. Nagib. 1972. <u>Experiments on Management of Free Stream Turbulence</u> NATO-AGARD, 598.

[13] Pfenninger W. <u>Recent Developments in the Field of Low Drag Boundary Layer Suction Research</u> AGARD, 262.

[14] Pfenninger, W., J. Bacon, and J. Goldsmith. 1967. Flow Disturbance Induced by Low-Drag Boundary Layer Suction Through Slots. <u>Physics of Fluids Supplement</u>, pp. S112-S114.

[15] Schlichting, H. 1968. <u>Boundary Layer Theory</u> 6th ed., New York: McGraw-Hill.

[16] Thomas, A.S.W., and K.C. Cornelius. 1982. Investigation of a Laminar Boundary-Layer Suction Slot. <u>AIAA Journal</u> 81-0194R 20, no. 6: 790-796.

[17] Thwaites, B. 1949. Approximate Calculations of the Laminar Boundary Layer. <u>The Aeronautical Quarterly</u> I (May): 245-280

[18] White, Frank M. 1979. <u>Fluid Mechanics</u> New York: McGraw-Hill Book Company.

[19] Surfer Access System Version 3.00 1987. Golden Software, Inc.

Appendix A

Boundary-layer Analysis

In searching for a good approximation for the boundary-layer thickness (δ), two factors must be considered. It must be determined how the axis-symmetrical contraction affects the boundary layer. With this informastion, an appropriate value for the inlet length (x_l) can be determined. Furthermore, it must be recognized that the flow in this experiment is not flow over a flat plate, but rather pipe flow. To predict confidently δ, the differences between these two types of flow must be explored.

Thwaites [17] developed a method to predict boundary-layer displacement thickness defined by

$$\delta^* = \int_0^\delta (1 - \frac{u}{U_o})dy$$

He shows that for accelerating fluid over a plate, the boundary-layer thickness can be evaluated through the relation:

$$U_o^6\theta^2 = .45\nu \int_0^x U_o^5 dx + \text{const.}, \qquad (A.1)$$

where U_o is the freestream velocity and θ is the momentum thickness. Thwaites [17, page 265] also proposed accompanying tables for H as a function of the velocity gradient (dU/dx), where $H = \delta^*/\theta$. In this case it is assumed that $dU/dx \approx 0$ at the slot and from Thwaites calculations for this condition, $H = 2.61$. The momentum

thickness at $x = 0$ is normally set to zero, and therefore, the constant in Eq. A.1 is set equal to zero.

Eq. A.1 is simplified by noting

$$U_o = \frac{UR^2}{r^2} ,$$

where U is the freestream velocity at the slot, R is the radius at the slot and $r(x)$ is the radius any given location. Therefore, both U and R are constant with respect to x. Furthermore, $U_o^6 = U^6$, since Eq. A.1 is to be solved for conditions at the slot. Solving Eq. A.1 for θ^2 and simplifying as described leads to

$$\theta^2 = \frac{.45\nu R^{10}}{U} \int_0^x \frac{1}{r^{10}} dx . \qquad (A.2)$$

The integral in Eq. A.2 was evaluated as follows:

$$\int_0^{x_s} \frac{1}{r^{10}} dx = \int_0^{bc} \frac{1}{r^{10}} dx + \int_{bc}^{ec} \frac{1}{r^{10}} dx + \int_{ec}^{s} \frac{1}{r^{10}} dx . \qquad (A.3)$$

Here the subscripts bc means "beginning of contraction" and ec means "end of contraction." The value of

$$\int_0^{x_s} \frac{1}{r^{10}} dx$$

is very insensitive to the exact location of the lower limit of integration. For this calculation the lower integration limit will be set at the end of the honeycomb in the settling chamber. By substituting values into Eq. A.3, it can be rewritten as follows:

$$\int_0^{115} \frac{1}{r^{10}} dx = \int_0^{76} \frac{1}{7.62^{10}} dx + \int_{76}^{105} \frac{1}{r^{10}} dx + \int_{105}^{115} \frac{1}{1.27^{10}} dx , \qquad (A.4)$$

where all values are in centimeters.

By evaluating the terms in Eq. A.4, and substituting into Eq. A.2, one finds:

$$\theta^2 = \frac{.45 \times 10^{-2}}{U} (2 \times 10^{-6} + \int_{bc}^{ec} \frac{1}{r^{10}} dx + 10) . \qquad (A.5)$$

Clearly, the first term on the right side of Eq. A.5 involving integration of the velocity in the settling chamber is insignificant compared to the term that accounts for the velocity in the 10 cm leading up to the slot. The middle term, which accounts for the accelerating fluid in the contraction, was evaluated by fitting a straight line between 16 incremental points along a template of the contraction. The integral of each straight line was then evaluated analytically and led to the result:

$$\int_{76}^{105} \frac{1}{r^{10}} dx = 1.33 \,.$$

This implies that the equivalent length for the flow along a flat plate (x_l) is equal to 11.33 cm. Additionally,

$$\theta = \frac{2.26 \times 10^{-4}}{\sqrt{U}} \,,$$

where U is in m/s. Thus, by Thwaites' method, for $U = 4$ m/s, $\delta^* = .294$ mm. Using the x_l derived above and the approximation [1]

$$\delta \approx \frac{5.0 x_l}{\sqrt{Re_x}} \,,$$

where δ is the distance at which $u = .99U$, the thickness δ is .84 mm. Assuming the flow to be similar to flow over a flat plate, as has been done throughout this section, it can be shown that $\delta \approx 3\delta^*$. Accordingly, δ^* as computed in this way is about equal to the value obtained in the foregoing method. With the Blasius approximation, values for δ were calculated as a function of U and are shown in Table. A.1.

Thwaites' method, based on two-dimensional theory, is valid for the flat plate, but not necessarily applicable to pipe flow. Therefore, to be thorough, it is necessary to explore some axis-symmetrical models of pipe flow, especially as they relate to

---

[1]This result was obtained from the Blasius equation, which was solved numerically by L. Howarth and presented by H. Schlichting [15, pages 125-130].

U (m/s)	1	2	3	4	5	6
δ (mm)	1.68	1.19	.97	.84	.75	.69

Table A.1: Theoretical Boundary-Layer Thickness.
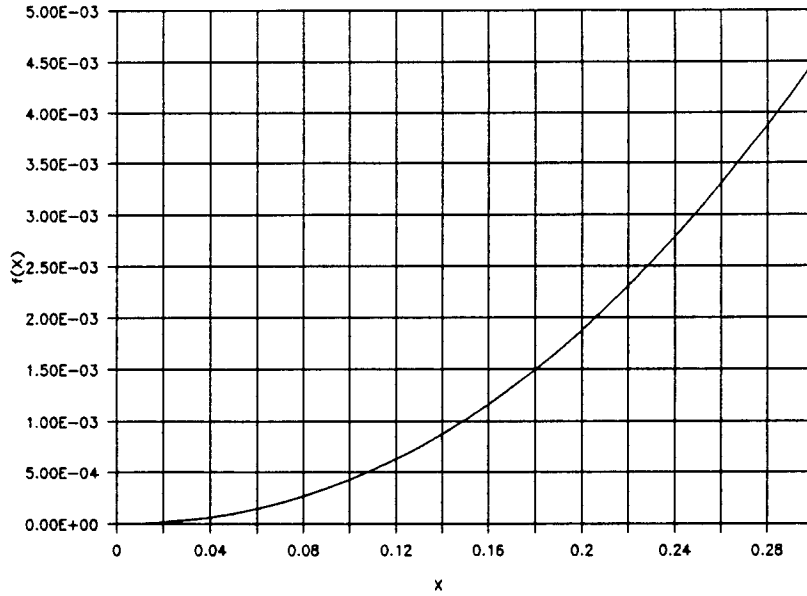
Figure A.1: Inlet length in a pipe by Schiller's method.

inlet length. S. Goldstein [6, pages 301–302] uses a simplified form of Schiller's method to predict inlet length in a pipe. He defines

$$\chi = \frac{U}{U_m} - 1$$

and sets $Re_d = \frac{U_m d}{\nu}$. He then derives the following result

$$f(\chi) = \frac{2x}{Re_d d},$$

and develops a lengthy relationship between $f(\chi)$ and χ, which is plotted in Fig. A.1.

With this design and $x_l = 11.3$, $f(\chi)$ varied from 3×10^{-4} to 5×10^{-5} as the pipe flow rate varied from 1 m/s to 6 m/s, respectively. Fig. A.1 shows that

$\chi \leq .08$, which implies that $\frac{U}{U_m} \approx 1$ and indicates that the flow is far from being fully developed. Further results from Nikuradse [6, pages 303-304] show that $\frac{U(.9r)}{U_m} \approx 1$, where U(.9r) is the velocity at a pipe radius of $.9r$. These results show that the two-dimensional results should be valid since the pipe flow is in such an undeveloped state at the slot. Additionally, they lend credence to the earlier assumption that $dU/dx \approx 0$, when $r =$ constant.

S. Barker and D. Gile [1, pages 151-153] investigated the pipe inlet flow phenomena in great detail, both experimentally and theoretically. They assumed, as in this paper, that the favorable pressure gradient of the contraction would greatly thin the boundary layer. This eliminates any dependence on the flow upstream of the constant diameter test section. The results from Thwaites' method seemed to justify this assumption. S. Barker and D. Gile measured the velocity profiles in the test section at various azimuth angles and found the boundary-layer thickness to vary by as much as 50% over the pipe circumference. However, they also found that the thickness averaged over the circumference was almost exactly that predicted by the two-dimensional theory, lending further credence to the previous calculations in this section.

Appendix B

Accuracy of the Results

The precision with which the materials were manufactured and the errors associated with the instrumentation have been discussed in Chapter 3. Those errors will now be applied to the data. In this experiment C_d is presented as function of Re_w, Re_x, (U/u_s) and S_a. In order to evaluate the error in C_d, the following approach is used:

$$dC_d = d\frac{1}{\sqrt{C_p}} = d\sqrt{\frac{\frac{1}{2}\rho u_s^2}{\Delta p}} \,, \tag{B.1}$$

where dC_d is the experimental error. As before, it is assumed that ρ is a known constant. Therefore,

$$dC_d = \sqrt{\frac{1}{2}\rho}\{\frac{1}{\sqrt{\Delta p}}du_s + u_s d(\frac{1}{\sqrt{C_p}})\} \tag{B.2}$$

or

$$dC_d = \sqrt{\frac{1}{2}\rho}(\frac{1}{\sqrt{\Delta p}}du_s - \frac{u_s}{\Delta p^{3/2}}d\Delta p) \,. \tag{B.3}$$

In order to evaluate dC_d, both du_s and $d\Delta p$ must be determined. The error, du_s was evaluated as follows:

$$du_s = d(\frac{q_s}{2\pi r w}) \,. \tag{B.4}$$

After some algebra, Eq. B.4 becomes

$$\frac{du_s}{u_s} = \frac{1}{V}dV - \frac{1}{w}dw - \frac{1}{r}dr - \frac{1}{t}dt \,, \tag{B.5}$$

	Error	Term	High	Low
dw	$\pm.03$ mm	$\frac{1}{w}dw$	$\pm.23$	$\pm.06$
dr	$\pm.1$ mm	$\frac{1}{r}dr$	$\pm.01$	$\pm.01$
dt	±1sec	$\frac{1}{t}dt$	$\pm.067$	$\pm.004$
dV	$\pm.02$ liter	$\frac{1}{V}dV$	$\pm.01$	$\pm.01$
dz	±2 mm	$\frac{1}{z}dz$	$\pm.2$	$\pm.002$

Table B.1: A comparison of the different error terms

where t is the time it takes to fill V, the volume of the 2000 ml flask, while

$$d\Delta p = d(z\rho g) = \rho g dz \,, \tag{B.6}$$

where z is the reading from the manometer.

By combining the result of Eqs. B.4 and B.6, Eq. B.3 can be rewritten as

$$\frac{dC_d}{C_d} = \frac{1}{V}dV - \frac{1}{w}dw - \frac{1}{r}dr - \frac{1}{t}dt - \frac{1}{z}dz \,. \tag{B.7}$$

The values for dw and dz were discussed previously in Chapter 3. Following a similar argument as the one used to derive dw, it is estimated that $dr = .1$ mm.

The error associated with q_s is evaluated in the following manner. The value for dt is the random error associated with stopping the clock when the water reached the two-liter mark, which is estimated to be ±1 sec. The value for dV, on the other hand, is the error associated only with the calibration of the two-liter flask. It was previously determined that $\frac{1}{V}dV < .01$.

The values for the different terms in Eq. B.7 are compared to each other in Table B.1. It is clear that the precision of the slot-width measurement is the most important variable, followed by the accuracy of the manometer readings.

Eq. B.7 is solved for the full range of values for each of its terms, noting that the maximum values for z and t do not occur simultaneously. These results are given in Table. B.2. As expected, the large errors are associated with low slot flow, hence small manometer readings, and narrow slot width.

A separate categorization was created primarily because the slot width could not be measured with great precision. In Table B.2 this error is referred to as the *relative* error. This is the error between data points for a given slot width and, therefore, does not take into account the error associated with measuring the slot width.

When $\frac{dC_d}{C_d}$ is expressed in *relative* terms, the data do not seem so unreliable. Recomputing dC_d with Eq. B.7 by setting the error associated with dw to zero, one gets much more pleasant results (see Table. B.2).

Quantifying the error associated with Re_w is done in a similar manner. Set

$$dRe_w = d(\frac{u_s w}{\nu}) = \frac{u_s w}{\nu}(\frac{1}{w}dw + \frac{1}{u_s}du_s - \frac{1}{\nu}d\nu) \,. \tag{B.8}$$

Eq. B.8 can be further simplified by expanding du_s, as done previously. This leads to

$$\frac{dRe_w}{Re_w} = (\frac{1}{V}dV - \frac{1}{\nu}d\nu - \frac{1}{r}dr - \frac{1}{t}dt) \,. \tag{B.9}$$

Note that dRe_w is not a function of w. All of these terms, except $\frac{1}{\nu}d\nu$ have been quantified in Table B.1. For simplicity it will be assumed that $\frac{1}{\nu}d\nu = .02$, since the viscosity of the water used was never actually checked, and it may have contained some impurities affecting the viscosity.

The results in Table. B.2 were obtained by substituting numerical values for the terms in Eq. B.9. Notably, the maximum error in Re_w occurs at the highest slot flow rates.

	(w = .13 mm)		(w = .5 mm)		relative	
	low q_s	high q_s	low q_s	high q_s	low q_s	high q_s
$\frac{dC_d}{C_d}$	±.46	±.34	±.28	±.15	±.2	±.09
$\frac{dRe_w}{Re_w}$	±.04	±.11	±.04	±.11	±.04	±.11
$\frac{dRe_x}{Re_x}$	±.05		±.05		±.05	
$\frac{d(U/u_s)}{U/u_s}$	±.3	±.35	±.12	±.18	±.06	±.12

Table B.2: Error values for the dimensionless coefficients

Following the same procedures as delineated previously,

$$dRe_x = d\frac{Ux_l}{\nu} = \frac{Ux_l}{\nu}(\frac{1}{x_l}dx_l + \frac{1}{U}dU - \frac{1}{\nu}d\nu) \,. \tag{B.10}$$

Re_x is normally associated with flows over a flat plate and is useful for determining the point of transition to turbulence. The present flow, although in some respects analogous to flow over a flat plate, is different. Therefore, Re_x should be used for rough comparisons only. For a more complete discussion and analysis of Re_x, see Appendix A.

Since, U_m is approximately equal to U and is simpler to measure than U, it will be evaluated. Eq. 5.4 leads to

$$\frac{dU_m}{U_m} = (\frac{1}{C}dC + \frac{1}{f}df) \,, \tag{B.11}$$

where C is a constant determined by the manufacturer and the size of the pipe, and in this case is equal to 0.2229. The manufacturer of the flow meter estimates that $\frac{1}{C}dC \approx 0.02$. Since values for the frequency (f) were taken with each data point, a statistical base could be built. The standard deviation was determined for some of these groups of data in order to better evaluate the accuracy of f. From this it was determined that $\frac{1}{f}df \leq 0.015$ and on the average, $\frac{1}{f}df \approx 0.001$. This implies

that there is little experimental error associated with f because so many values were taken.

Eqs. B.10 and B.11 can be combined and rewritten as

$$\frac{dRe_x}{Re_x} = \frac{1}{x_l}dx_l + \frac{1}{C}dC + \frac{1}{f}df - \frac{1}{\nu}d\nu \ . \tag{B.12}$$

Notably, dRe_x/Re_x is not a function of slot width or flow rate.

Following the same procedure as before for analysis of $\frac{d(U/u_s)}{U/u_s}$ leads to:

$$\frac{dU/u_s}{U/u_s} = \frac{1}{C}dC + \frac{1}{f}df + \frac{1}{r}dr + \frac{1}{t}dt - \frac{1}{V}dV + \frac{1}{w}dw \ . \tag{B.13}$$

All of these terms have been discussed previously and values for $\frac{d(U/u_s)}{U/u_s}$ are given in Table B.2.

The final coefficient to evaluate is S_a, which can be expressed as:

$$dS_a = \frac{2g}{U^2}[dz_o - dz - \frac{2}{U}(z_o - z)] \ . \tag{B.14}$$

For this coefficient the error estimation is clearer when not expressed as a ratio. Eq. B.14 indicates that dS_a decreases with increasing U. Therefore, the largest errors occur at low pipe flow. The error in S_a can be as great as 0.4 at low U, and 0.02 at high U. At a pipe flow rate of 3 m/s, $dS_a = 0.07$.